The Influence of Electrical Fields on Grain Growth in SiC

Amir Gabay

The Influence of Electrical Fields on Grain Growth in SiC

Research Thesis

In Partial Fulfillment of the

Requirements for the Degree of

Master of Science in Material Science and Engineering

Amir Gabay

Submitted to the Senate of

the Technion – Israel Institute of Technology

Nisan 5775 Haifa April 2015

The research thesis was done under the supervision of Prof. W.D. Kaplan in the Department of Materials Science and Engineering.

Acknowledgements

I would like to thank my supervisor Prof. Wayne D. Kaplan for mentoring me, believing in me and encouraging me during the research, and for teaching me how to research and how the world of science works.

I would like to thank the Metal-Ceramic Interface Group for their help and support, Hadas Sternlicht, Eran Gros, Ran Akiva, Dana Benes, Ruth Moshe, Galit Atiya, Hadar (Bratt) Nahor Oren Shani and Tomer Shtien, for helping me throughout the research in various ways.

I want to thank Uri Veinberg and Rachel Marder for help with the research.

I want to thank Prof. Nahum Frage and PHD Shmuel Hayun for helping with conducting of the SPS experiments.

Table of Contents

1 Introduction 1

2 Literature Survey 2

2.1 Sintering 2

2.1.1 Sintering Definition 2

2.1.2 Sintering and Mass Transfer 3

2.1.3 Solid-State Sintering Stages 4

2.1.4 Sintering Additives 4

2.1.5 Sintering Requirements 5

2.2 Powder Processing 5

2.3 Silicon Carbide 6

2.3.1 Silicon Carbide Properties 6

2.3.2 Silicon Carbide Uses 7

2.4 Spark Plasma Sintering (SPS) 7

2.4.1 Origin of the Name 7

2.4.2 SPS Components 8

2.4.3 Advantages and Disadvantages of SPS 9

2.4.4 Problems in Temperature Measurement during SPS 10

2.5 Grain Growth 11

2.6 Grain Boundary Mobility 13

2.7 Effective Grain Boundary Mobility 13

2.8 Abnormal Grain Growth 14

2.9 The Influence of Electric Field on Grain Growth and on Effective Grain Boundary Mobility....15

2.10 Silicon Carbide in SPS....17

3 Research Goals....19

4 Experimental Methods....20

4.1 Sintering....20

4.1.1 Powder Preparation....20

4.1.2 Green Body Preparation....21

4.1.3 Sintering....21

4.1.4 Annealing....22

4.1.5 Furnaces....22

4.2 Sample Preparation for Characterization....23

4.3 Characterization....23

4.4 Grain Size Measurements....23

4.5 Effective Grain Boundary Mobility....23

5 Results....24

5.1 SiC Microstructure after Convectional Sintering at 2100ºC....24

5.2 SiC Microstructure after Convectional Annealing at 2100ºC....24

5.3 Effective Grain Boundary Mobility under Conventional Annealing....25

5.4 SiC Microstructure after SPS Annealing At 2100ºC....26

5.5 Effective Grain Boundary Mobility under SPS Annealing at 2100ºC....28

5.6 SiC Microstructure after SPS Annealing At 1800ºC....31

5.7 Aspect Ratio as a Function of Annealing Time 33

5.8 Aspect Ratio as a Function of Grain Size 36

5.9 Grain Growth Orientation as a Function of Electrical Field Direction 38

6 Discussion 39

6.1 The Effective Grain Boundary Mobility of SiC in Conventional and SPS Annealing 39

6.2 The Influence of Electrical Field on Grain Growth 40

6.3 The Influence of Electrical Field on Grain Orientation 41

6.4 Anisotropy 41

6.4.1 Possible Reasons for Anisotropy 41

6.4.2 Possible Extrapolation of the Aspect Ratio as a Function of Grain Size 42

7 Summary and Conclusions 44

8 Recommendations for Future Work 45

1. References 46

תודות V

תקציר I

List of Figures

Figure 1: Schematic illustration of the densification process, where the replacement of solid-vapor surfaces with solid-solid surfaces occurs. 2

Figure 2: Schematic illustration of coarsening, where the reduction of solid-vapor surface area is driven by the minimization of surface energy. 3

Figure 3: Schematic illustration of sintering mass transfer mechanisms, where Δp is evaporation condensation, Ds is surface diffusion, D_{GB} is grain boundary diffusion, Dl is volume diffusion and η is creep flow. 3

Figure 4: Schematic illustration of the three solid-state sintering stages: (A) Neck growth; (B) Continuous pores; and (C) Closed pores. 4

Figure 5: Polytypes/polymorphs of SiC, marked as xH/xR/xC where H/R/C represents hexagonal , rhombohedral or cubic, respectively and x is the number of (0001) or (001) planes in the unit cell. 6

Figure 6: Schematic illustration of the first suggested physical mechanism for spark plasma sintering. 8

Figure 7: Schematic illustration of the major components of SPS. 9

Figure 8: Growing difference between the thermocouple reading (from the surface of the sample) and the pyrometer on the outer surface of the die (reproduced from [13]). 11

Figure 9: Schematic illustration showing the TLK model, the sequence of the different states of an atom during grain boundary migration. [17]. 12

Figure 10: Illustration of polycrystalline material, where a grain with more than six neighbors will grow while grain with less than six neighbors wills shrinkage. Arrows indicating the direction of boundaries migrate [20].....15

Figure 11: Backscattered electron SEM micrographs of the microstructure of Yttria stabilized Zirconia (3Y-TZP) after annealing (a) without applying electric field and (b) after applying electric field. (Reproduced from [21]).....15

Figure 12: Grain growth kinetics of yttria stabilized zirconia (3Y-TZP) conventionally annealed (E0) and annealed in the presence of a constant electric field (Ea=18 V/Cm) showing grain growth retardation. (Reproduced from [21]) 16

Figure 13: Schematic of the thermal history of the specimens in the isothermal annealing tests without and with dc electric fields. (Reproduced from [21]).....16

Figure 14: Relative density ρ_r and mean linear intercept grain size d versus annealing time for t_a for the isothermal annealing of 3Y-TZP without and with an applied DC electric field E=18V/Cm (a) at 1300°C and (b) at 1400°C. (Reproduced from [21]) 17

Figure 15: Backscattered electron SEM micrograph of the microstructure of SiC after SPS with heating and cooling rate of 400°C/min and only 0-10 min dwell at 2050°C under vacuum of 1.3 h Pa and uniaxial pressure of 69 MPa (reproduced from [4]).....18

Figure 16 Backscattered electron SEM micrograph of the microstructure of SiC after sintering. 24

Figure 17 Backscattered electron SEM micrograph of the SiC microstructure after 4 hours conventional annealing at 2100ºC. 25

Figure 18: SiC grain size distribution after 4 hours of conventional annealing at 2100ºC. 25

Figure 19: Grain growth kinetics of SiC conventionally annealed at 2100ºC. 26

Figure 20: Backscattered electron SEM micrograph of SiC after 16 min of annealing at 2100ºC using SPS. 27

Figure 21: SiC grain size distribution after 16 min of annealing at 2100ºC using SPS. 27

Figure 22: Backscattered electron SEM micrographs of SiC after 32 min of annealing using SPS at 2100ºC. 28

Figure 23: Backscattered electron SEM micrograph of SiC microstructure after 120 min of annealing using SPS at 2100ºC. 28

Figure 24: Grain growth kinetics of SiC in SPS at 2100ºC using (a) a linear fit to the entire population of grain sizes; (b) a linear fit to small grains only; (c) a parabolic fit to the entire grain size population; and (d) a parabolic fit to the small grains. 30

Figure 25: Backscattered electron SEM micrograph of SiC microstructure after 16 min of SPS annealing at 1800ºC 31

Figure 26 Grain growth kinetics of SiC in SPS at 1800ºC. 32

Figure 27: Grain aspect ratio as a function of annealing time in SPS at 2100ºC for (a) 0 min annealing (b) 16 min annealing and (c) 32 min annealing. 34

Figure 28: Aspect ratio as a function of annealing time for conventional and SPS annealing at 2100ºC. 35

Figure 29: Aspect ratio as a function of grain size in conventional and SPS annealing at 2100ºC. 37

Figure 30: Backscattered electron SEM micrographs of SiC microstructure (a) perpendicular to the electrical field and (b) parallel to the electrical field. 38

Figure 31: Schematic illustration of current (in red) which flows mainly through the die and through the grain boundaries in SPS. .....**שגיאה! הסימניה אינה מוגדרת.**

Figure 32: Schematic illustration of constant aspect ratio as a function of time; constant velocity of grain boundaries, with different velocities for each boundary. 42

Figure 33: Schematic illustration of changing aspect ratio as a function of time; acceleration (different accelerations) of grain boundaries. 42

Figure 34: Schematic illustration of possible extrapolation of the graph of aspect ratio as a function of grain size in conventional and SPS annealing. 43

List of Tables

Table 1: SiC 6H powder (0.7μm, Electro abrasives LLC) used for the first sintering. 20

Table 2: Raw data of Figure 18.....26

Table 3: Raw data of Figure 23 (a) and (c). 30

Table 4: Raw data of Figure 23 (b) and (d). 31

Table 5: Raw data of Figure 25.....32

Table 6 Effective grain boundary mobility of SiC annealed by conventional furnace and SPS. 33

Table 7: Raw data of Figure 27.....36

Table 8: Raw data for Figure 28. 37

Abstract

During (electromagnetic) field assisted sintering a green body is exposed to an electric field and elevated temperature. The exposure to an electric field causes faster sintering rates compared to conventional sintering methods. Assuming the microstructure of the sintered body is controlled, this process can result in improved material properties (e.g. strength, transparency, and conductivity). However, there is a debate in the literature regarding the mechanism(s) of electromagnetic field assisted sintering, and understanding the mechanism is critical to implementation of the method.

This research focuses on the influence of electromagnetic fields on grain growth, rather than on sintering. As a model system, SiC was first sintered using conventional pressure-less sintering at 2100°C under He. Samples from the sintered bodies then underwent annealing treatments in the same conventional furnace, and the grain size as a function of annealing time was characterized. In parallel, identical samples were annealed using a spark plasma sintering (SPS) device without pressure, at identical and at lower temperatures, and the grain size as a function of annealing time was characterized.

From these experiments, the grain boundary mobility of SiC at 2100°C under conventional heating versus SPS was determined. Conventional heating resulted in a grain boundary mobility of $3.53 \cdot 10^{-17}$ m^2/sec. SPS resulted in a grain boundary mobility of $1.36\text{-}4.79 \cdot 10^{-14}$ m^2/sec at 2100°C and $6.22 \cdot 10^{-17}$ m^2/sec at 1800ºC. While the aspect ratio of grains as a function of time during conventional and SPS annealing showed different trends, the aspect ratio as a function of grain size after conventional versus SPS annealing showed the same trend. This

indicates that the same (or similar) mechanism(s) which promotes rapid sintering during SPS also significantly increases the rate of grain growth.

List of Symbols and Acronyms

T_m	Melting Temperature
γ	Surface/interface energy
A	Total surface
r_1, r_2	The radii of curvature perpendicular with each other at the interface
k	Curvature
T	Temperature
P	Pressure
t	Time
SEM	Scanning electron microscope
pH	Power of hydrogen
°C	Celsius
ρ	Density
wt.%	Weight percent
P	Pressure
SPS	Spark Plasma Sintering
s.e.m	Standard error of the mean
s	Standard deviation
N	Number of measurements
γ_{SV}	Solid-vapor surface energy
γ_{LV}	Liquid-Vapor surface energy
γ_{GB}	Grain-boundary energy

1 Introduction

Due to its relatively light weight, high strength and high toughness, SiC is used in abrasives and cutting tools, and in ballistic armor. While its single crystalline form has applications as a semi-conductor substrate, it is mostly used in a polycrystalline form [1]. SiC can be sintered using different methods, but grain growth usually occurs and controlling the grain size and morphology is important for optimization of the mechanical properties. Recently, field assisted sintering methods were applied to SiC, where one reason was the reduced sintering temperature compared to conventional sintering [2,3]. The hope is that field assisted sintering will result in lowered sintering temperatures in addition to reduced times, and finer microstructures.

While spark plasma sintering (SPS) has been explored to sinter SiC to full density, its influence on grain growth has not been quantified [4]. Recent studies argue that electric fields retard grain growth in yttrium stabilized zirconia (YSZ) [5], and others argue that flash sintering can reduce grain growth to zero [6]. While there is no doubt regarding the presence of an electric field in SPS, its influence on grain growth has not been quantified. A quantitative way to follow changes in grain growth rates is to measure the grain boundary mobility [7]. The goal of this work was to evaluate the grain boundary mobility of SiC as a result of conventional annealing compared to annealing using SPS.

2 Literature Survey

2.1 Sintering

2.1.1 Sintering Definition

Sintering is a process by which a powder or a green body is transformed into a dense polycrystalline matrix. The driving force for sintering is the reduction of the total surface/interfacial energy which can be express as [8]:

$$\Delta(\gamma A) = \Delta\gamma A + \gamma\Delta A \quad (1)$$

where, γ is the surface/interface energy of a particle, A is the total interface area, γA is the total interfacial energy of the compact powder. The interfacial energy of the compact powder $\Delta(\gamma A)$ can be lowered by densification , as demonstrated in Figure 1, that reduces surface energy by replacing solid-vapor surfaces with solid-solid surfaces (interfaces), and if thermally activated, by coarsening (grain growth), as demonstrated in Figure 2, that is driven by the minimization of interface energy. Unlike the densification process, grain growth is mostly undesirable.

The temperature that sintering usually occurs is in the range of $0.5T_m < T < 0.8T_m$, where T_m is the melting temperature.

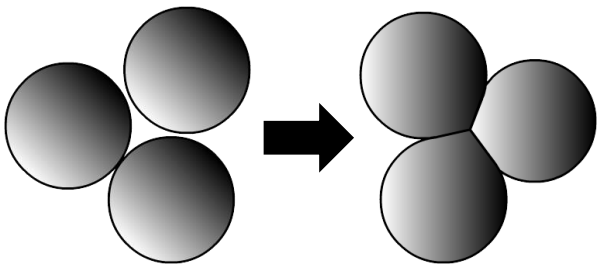

Figure 1: Schematic illustration of the densification process, where the replacement of solid-vapor surfaces with solid-solid surfaces occurs.

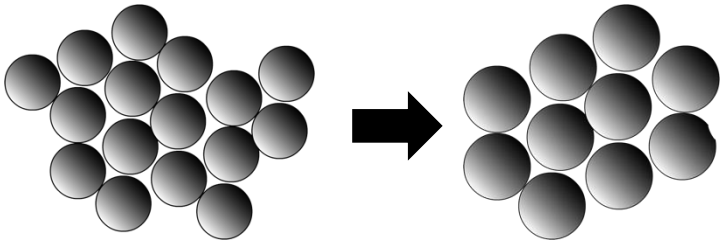

Figure 2: Schematic illustration of coarsening, where the reduction of solid-vapor surface area is driven by the minimization of surface energy.

2.1.2 Sintering and Mass Transfer

In order for sintering to occur, there is a need for mass transfer. There are several ways for mass to do that as demonstrated in Figure 3:

1. Evaporation from the solid-vapor surface and condensation around the neck between the grains;
2. Surface diffusion;
3. Volume diffusion;
4. Grain boundary diffusion;
5. Creep.

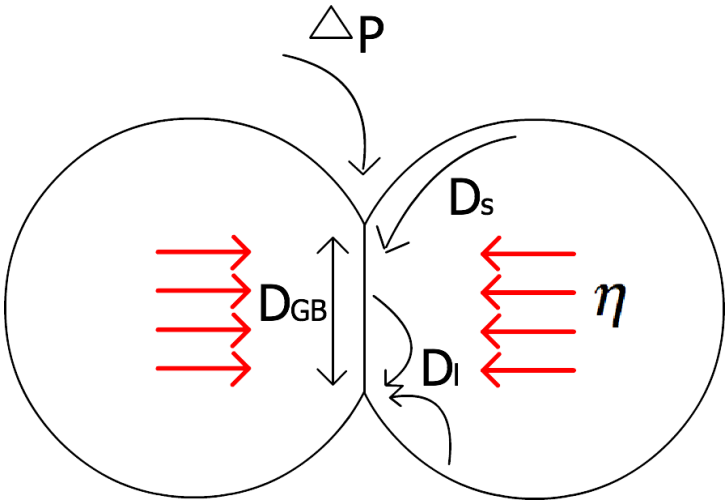

Figure 3: Schematic illustration of sintering mass transfer mechanisms, where Δp is evaporation condensation, Ds is surface diffusion, D_{GB} is grain boundary diffusion, Dl is volume diffusion and η is creep flow.

2.1.3 Solid-State Sintering Stages

One state of sintering is solid-state sintering. In this process the matter during the entire process is in the solid-state. Solid-state sintering can be divided into 3 main stages as demonstrated in Figure 4:

1. Neck growth: Initial attachment of the separated powder or green body particles to each other.
2. Continuous pores: In this stage the pores are connected to each other.
3. Closed pores: In this stage the pores are closed and disconnected from each other. Due to relatively small amount of free surface, densification is limited to grain boundary diffusion that is relatively slow in comparison with surface diffusion.

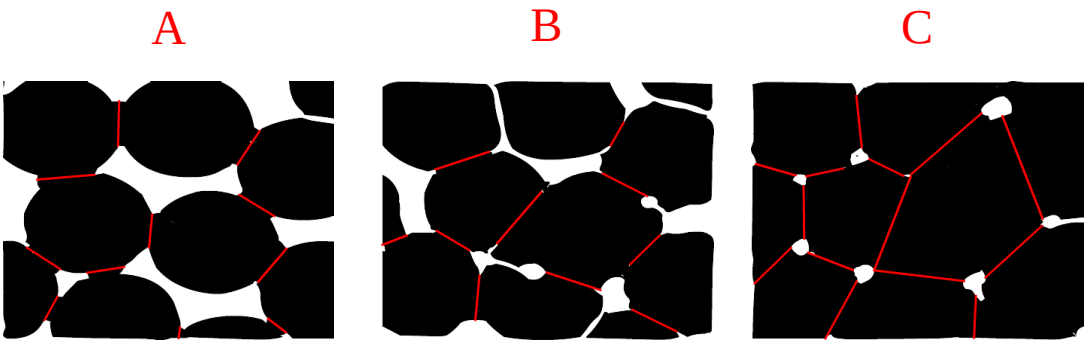

Figure 4: Schematic illustration of the three solid-state sintering stages: (A) Neck growth; (B) Continuous pores; and (C) Closed pores.

2.1.4 Sintering Additives

In most of the cases, sintering additives are added to the starting powder for the sintered body in order to improve the sintering process and improve the final microstructure. The influence of additives on sintering differs with the kind of the additive and its interaction with the sintered matter. Sintering additives can decrease the required sintering temperature, can affect the final microstructure, can form liquid phases, can change diffusion coefficients,

and as a result of some of the influences above can limit grain growth by changing grain boundary mobility [9], a desirable phenomenon in many cases, because limitation of grain growth and as a result a fine microstructure may result in better properties such as higher strength and higher transparency.

2.1.5 Sintering Requirements

To summarize the above, in order for sintering to occur, activation energy is required, e.g. thermal and/or pressure to allow for mass transport. In most cases, sintering requires a method by which surface annihilation continues while grain boundary annihilation is inhibited.

2.2 Powder Processing

Prior to sintering, powder processing is required. Powder processing can result in a powder that after pressing will yield a relatively strong and dense green body, and in turn a better sintered body. First, in order to break powder agglomerates that can decrease the density of the green body, the powder is mixed in a fluid medium (slip) with a dispersant (deflocculant), which results in a dispersed suspension. Due to high specific surface area of the initial powder, agglomerates can easily form, and the addition of a deflocculant is important because it breaks agglomerates by changing the pH of the slip from that of the isoelectric point of the particle [10], or reduces the effective surface tension of the powder particles, thus decreasing the inter-particle attraction forces. The next step after the slip production is ball-milling, where SiC balls mechanically break the agglomerates along with the dispersive effect of the deflocculant. After this process, the slip is dried, sieved and pressed to a green body.

2.3 Silicon Carbide

2.3.1 Silicon Carbide Properties

Silicon carbide is a ceramic with covalent bonds between silicon and carbon. SiC has a relatively low theoretical density (3.21 gr/cm^3), and a relatively high flexural strength of 550 MPa, a fracture toughness of 3-5 MPa•m$^{1/2}$ and Young's modulus of ~460 GPa. SiC is a semiconductor [11].

SiC has two main polymorphs [12]: a Wurtzite structure named α-SiC, a cubic polymorph of a Zinc-blend structure named β-SiC and a hexagonal polymorph with over 250 different polytypes. The polytypes in SiC ordered in a one-dimensional sequence of SiC_4 (or CSi_4) layers of tetrahedra, linked through their vertices, without any variation in stoichiometry, along the [0001] axis of the unit cell as shown in Figure 5. The polytypes/polymorphs that are most common are 3C, 4H, 6H and 15R [13].

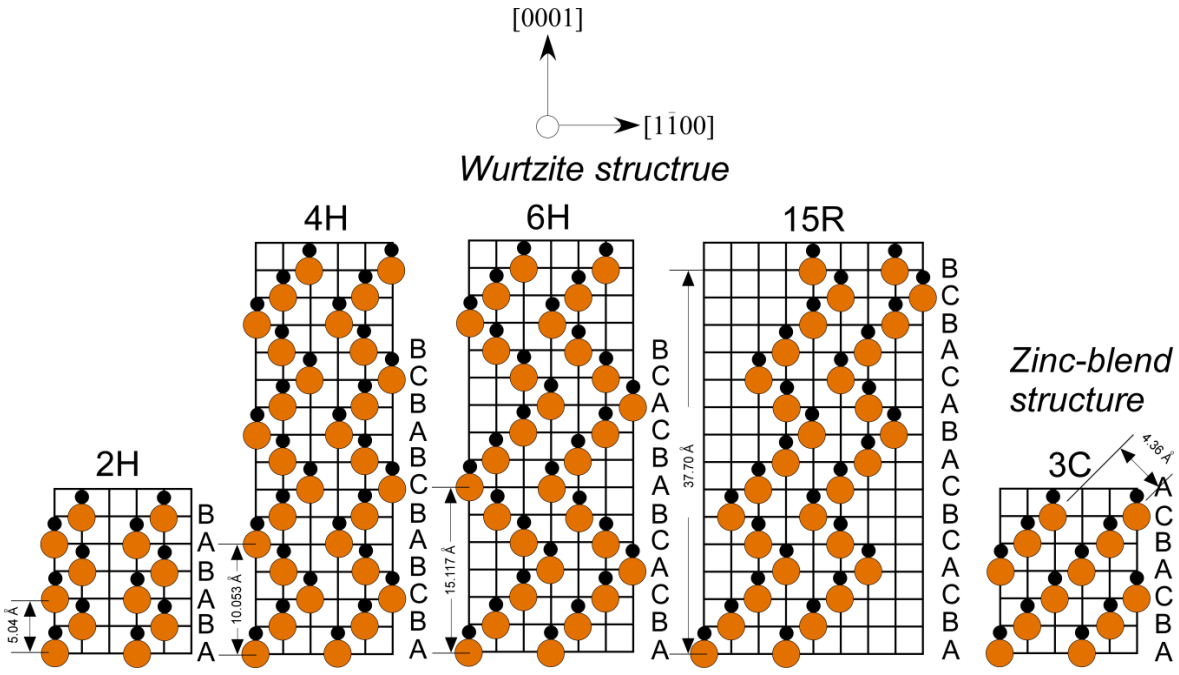

Figure 5: Polytypes/polymorphs of SiC, marked as xH/xR/xC where H/R/C represents hexagonal , rhombohedral or cubic, respectively and x is the number of (0001) or (001) planes in the unit cell.

2.3.2 Silicon Carbide Uses

Due to its relatively light weight and high strength SiC can be found in ballistic armor, in abrasive and cutting tools, and also in the semiconductor industry due to its semiconductor properties.

2.4 Spark Plasma Sintering (SPS)

2.4.1 Origin of the Name

Spark plasma sintering (SPS) is an unconventional sintering method by which the energy of the process is supplied by an electrical current flowing through a surrounding die, and through the sample itself [14]. This method is faster than conventional sintering methods. If in conventional sintering, the thermal treatment is a matter of hours, in SPS the whole process can last for only few minutes. The name, spark plasma sintering, was given by early researchers who believed, as demonstrated in Figure 6, that the applied voltage on the sample creates electric discharges through the gas between the particles and creates sparks, where the sparks were believed to ionize the gas and create a plasma, which in turn would enhance surface diffusion and therefore increase the sintering rate [15,16]. To date, no solid evidence for the presence of a plasma exists.

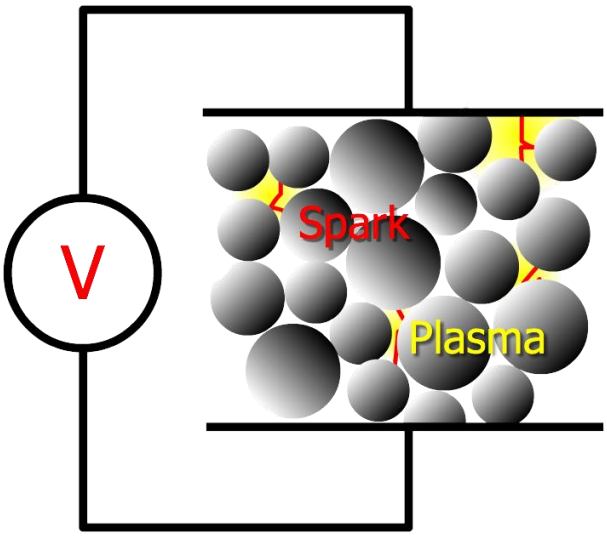

Figure 6: Schematic illustration of the first suggested physical mechanism for spark plasma sintering.

2.4.2 SPS Components

In SPS the sample, a powder or a green body is inserted into a graphite die, as shown in Figure 7, which is a good electrical conductor. The die is placed between two punches that are made of graphite. The die and the punches are placed in a vacuum chamber. Outside the system a pyrometer monitors the temperature of the die surface, and sometimes a thermocouple is used. The whole system is connected voltage source.

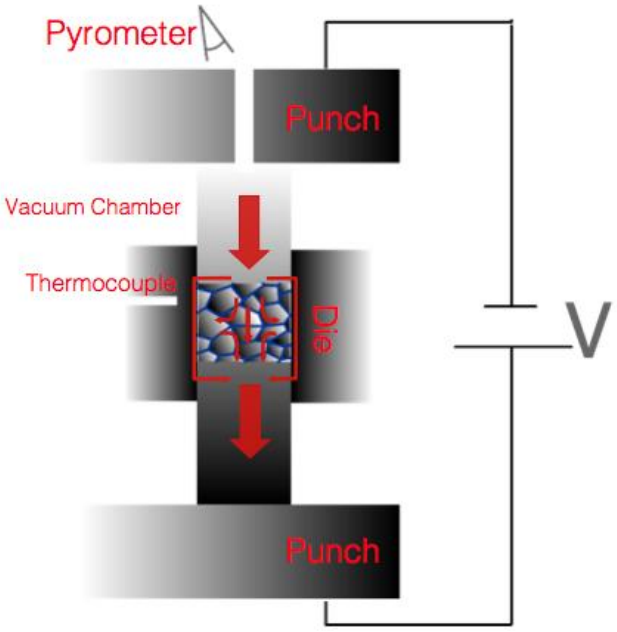

Figure 7: Schematic illustration of the major components of SPS.

The applied voltage creates electrical current that flows through the punches, and then through the die and the sample in parallel. The amount of current that flows though the sample depends on its electrical conductivity, where for insulators or semi-conductors most of the current flows through the die. The flowing current heats the die via Joule heating and therefore heats the sample.

2.4.3 Advantages and Disadvantages of SPS

The method of sintering using SPS results in a few advantages in comparison with conventional sintering. The advantages include [12]:

1. Very high heating rates, up to 1000ºC/min, due to the fast Joule heating of the die, in comparison with a maximum of 30°C/min for conventional sintering.
2. Low sintering temperatures $0.35T_m < T < 0.7T_m$ in comparison with $0.5T_m < T < 0.8T_m$ for conventional sintering.

3. Short sintering times; minutes in comparison with hours for conventional sintering.

On the other hand, the disadvantages include:

1. Limited size and shapes of the sample due to the limited size and shape of the die unlike in conventional sintering where the furnace chamber can come in various sizes.
2. Difficulties in measuring the temperature. The temperature in SPS is measured on the outer surface of the die and the sample temperature may be very different.
3. Inhomogeneous density for large samples due to inhomogeneous current densities and temperature gradients in the sample.
4. The sintering mechanism is not clear, which makes it harder to improve the use of this method.

2.4.4 Problems in Temperature Measurement during SPS

The temperature that the SPS system monitors is the one measured by a pyrometer that is monitoring the temperature on the outer surface of the die. Therefore, the actual temperature of the sample can be very different than what the SPS system indicates. Anselmi-Tamburini et al. measured the temperature on the surface of the sample by drilling a hole through the die and placing a thermocouple though it [17]. The simultaneous measurements of the temperature on the surface of the die by the pyrometer and on the surface of the sample by the thermocouple showed a constant gradient in the temperature in favor of the sample (i.e. the sample was hotter) that became larger as the temperature increased. At 1350ºC the thermocouple showed a constant difference of 150ºC in comparison with the pyrometer measurement that remained constant with time as shown in Figure 8.

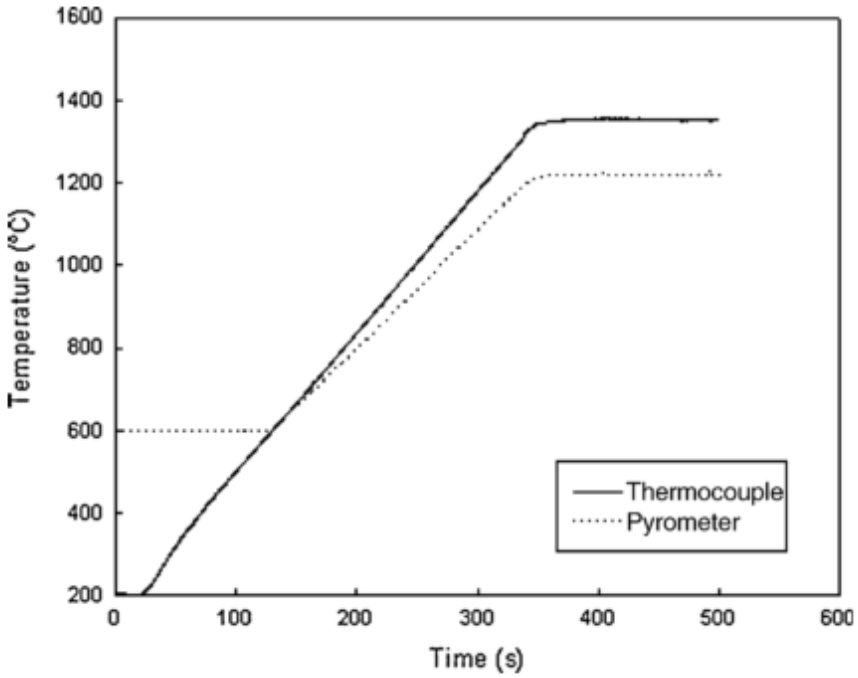

Figure 8: Growing difference between the thermocouple reading (from the surface of the sample) and the pyrometer on the outer surface of the die (reproduced from [13]).

2.5 Grain Growth

Grain growth is a process by which grain boundaries migrate in order to reduce the total amount of grain boundary area, which are more energetic in comparison with bulk energy, and thus grain growth reduces the total free energy of the system. Grain boundaries move via short term diffusion processes, where the atoms from one grain on one side of the boundary with a certain orientation, randomly jump towards the other side of the boundary and combine with the new orientation of the growing grain. Thus, grain boundary motion is in the opposite direction of the mean atomic flux [18].

When a grain is round, a curvature of the grain boundary can be defined. This grain boundary curvature creates a difference in the chemical potential, due to a pressure difference, between the two grains in favor of the concave grain and creates a local driving force for grain

boundary migration where atoms jumps from the concave grain with the higher chemical potential towards the convex grain with the lower chemical potential. This can be described:

$$\Delta P = \gamma_{GB}\left(\frac{1}{r_1}+\frac{1}{r_2}\right)=\frac{\alpha\gamma_{GB}}{G} \qquad (2)$$

where ΔP is the pressure difference between two adjacent grains, γ_{GB} is the grain boundary energy, α is a geometrical factor and G is the grain size.

Drag forces, which work in opposite to the driving force include intrinsic drag, solute drag, and pore drag, and at steady state drag forces balance the driving force.

Gleiter first suggested a mechanism for the migration of grain boundaries via the motion of grain boundary steps, using the terrace ledge kink (TLK) model [19]. In this model atoms along the boundary are believed to move via the motion of steps which form at triple junctions where an atom is detached from a kink site or a ledge (step) site of one grain on the grain boundary and jumps into a kink or ledge on the growing grain from the other side as shown schematically in Figure 9. While this model was based on the growth of a crystal from the liquid or vapor phase, Gleiter applied it for grain growth.

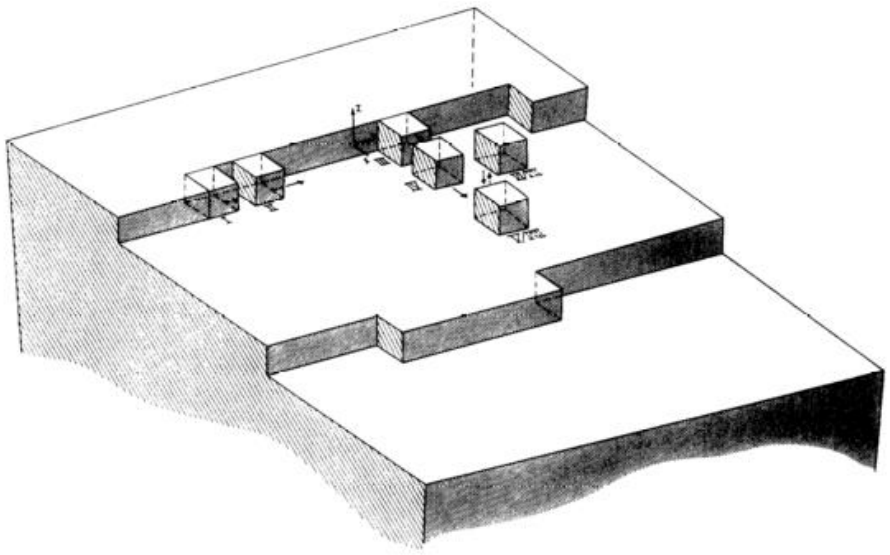

Figure 9: Schematic illustration showing the TLK model, the sequence of the different states of an atom during grain boundary migration. [17].

2.6 Grain Boundary Mobility

Grain boundary mobility (M_{GB}) is the velocity of a grain boundary (V_{GB}) normalized by the driving force for grain boundary migration (F_{GB}). It is convenient to normalize the velocity of the grain boundary and driving force to a new term called grain boundary mobility, because the velocity of the grain boundaries depends on the driving force and they both can change dramatically in the same system due to difference in grain size and curvature [7]:

$$M_{GB} = \frac{V_{GB}}{F_{GB}} \tag{3}$$

Grain boundary mobility is an important parameter to determine, because a change in the mobility can indicate a change in the mechanism. Grain growth can usually be described by an equation of the form:

$$\bar{G}_0^n - \bar{G}_t^n = K(t - t_0) \tag{4}$$

where $\bar{G}_0^n$ is the average grain size before annealing, $\bar{G}_t^n$ is the average grain size at time t , and the rate constant K can be converted to M_{GB} by:

$$M_{GB} = \frac{V_{GB}}{F_{GB}} = \frac{K}{n\gamma_{GB}\bar{G}^{n-2}} \tag{5}$$

where γ_{GB} is the grain boundary energy and n is the power law.

2.7 Effective Grain Boundary Mobility

After plotting a graph of average grain size as a function of annealing time and by using equations (4) and (5), the grain boundary mobility can be theoretically extracted. A major obstacle in determination of the mobility is the need to know the grain boundary energy. Like grain boundary mobility, grain boundary energy is mostly different in different

boundaries. Moreover, the measurement of grain boundary energy is a complicated task for a single boundary, and more so for all of the boundaries in a particular material system. Therefore, a more convenient term is the effective grain boundary mobility, which is the product of the grain boundary mobility and the grain boundary energy. Thus after calculation of the slope of the graph of average grain size as a function of annealing time using equation (4), the rate constant K (the slope) can be converted to the effective grain boundary mobility $\gamma_{GB}M_{GB}$ by:

$$\gamma_{GB}M_{GB} = \frac{K}{n\bar{G}^{n-2}} \tag{6}$$

2.8 Abnormal Grain Growth

Abnormal grain growth or exaggerated grain growth is where some specific grains grow significantly more than the rest of the grain population, in particular grains with more than six neighbors [20]. In general large grains are more stable than small grains due to less boundary per bulk, and therefore abnormal grains grow at the expense of normal grains, and necessarily exhibit a higher grain boundary mobility compared to normal grain growth, or the specific grain has boundaries with significantly less grain boundary energy. When a grain grows significantly more than its neighbors, it has a growing number of neighbors as shown in Figure 10, this phenomenon increases the curvature of each boundary between the large grain and its surroundings and will result in a rapid growth of the large grains at the expense of its neighbors. The detailed mechanism for abnormal grain growth is not fully understand. While a plot of grain size distribution of normal growth shows single peak, i.e. unimodal distribution, abnormal grain growth shows two peaks, i.e. bimodal distribution.

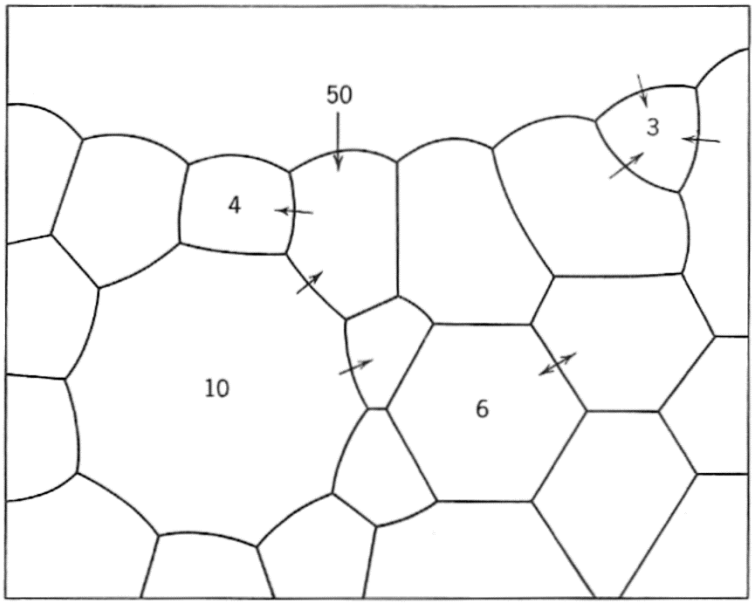

Figure 10: Illustration of polycrystalline material, where a grain with more than six neighbors will grow while grain with less than six neighbors wills shrinkage. Arrows indicating the direction of boundaries migrate [20]

2.9 The Influence of Electric Field on Grain Growth and on Effective Grain Boundary Mobility

Studies on the influence of electric fields on grain growth in different ceramics have been done, claiming retardation of grain growth under the influence of electric fields. Figure 11 demonstrates a result of the alleged influence of an electric field on grain growth in YSZ, claiming that the presence of the electric field during annealing caused retardation of grain growth [21,22].

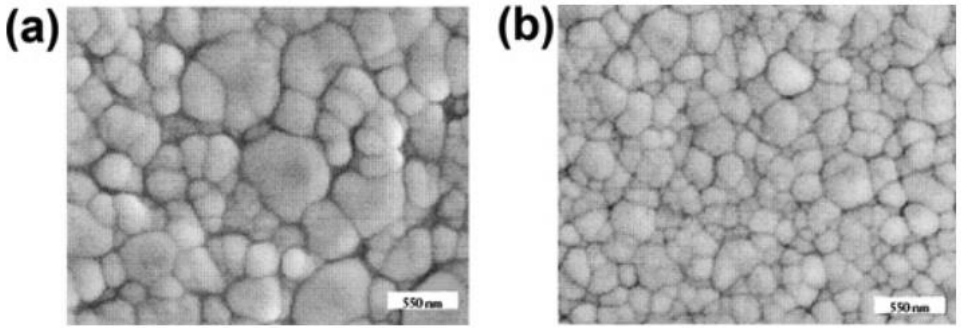

Figure 11: Backscattered electron SEM micrographs of the microstructure of Yttria stabilized Zirconia (3Y-TZP) after annealing (a) without applying electric field and (b) after applying electric field. (Reproduced from [21])

Figure 12 shows the grain growth kinetics with or without the presence of an electric field. The extracted effective grain boundary mobility from the graph are $4.68^{\bullet}10^{-17}$ m^2/sec in the presence of an electric field and $9.95^{\bullet}10^{-17}$ m^2/sec without the presence of an electric field.

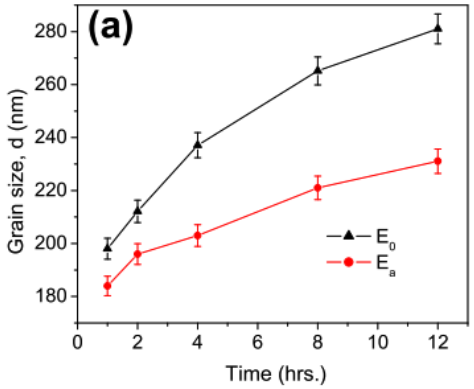

Figure 12: Grain growth kinetics of yttria stabilized zirconia (3Y-TZP) conventionally annealed (E0) and annealed in the presence of a constant electric field (Ea=18 V/Cm) showing grain growth retardation. (Reproduced from [21])

Other studies reports on zero grain growth during flash sintering [23]. A closer look at the annealing treatment program shown in Figure 13, shows that the alleged reported grain growth was measured only after bake-out, and not after full sintering.

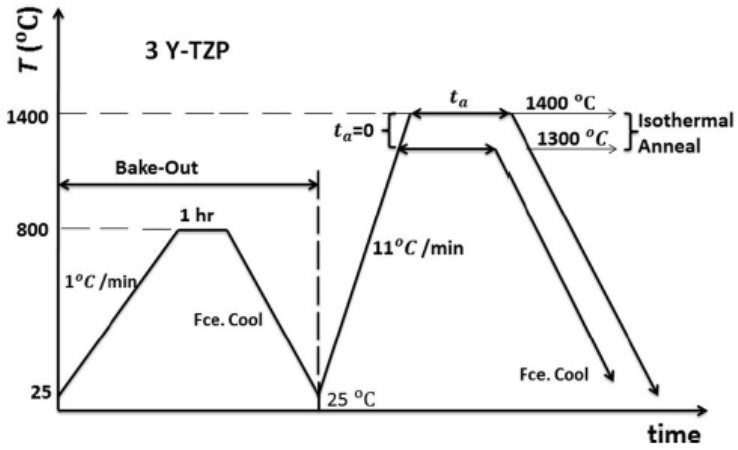

Figure 13: Schematic of the thermal history of the specimens in the isothermal annealing tests without and with dc electric fields. (Reproduced from [21])

Figure 14 clearly shows that grain growth was not the only process that occurred during this treatment, but sintering or densification has happened as well due to the change of the reported density in time.

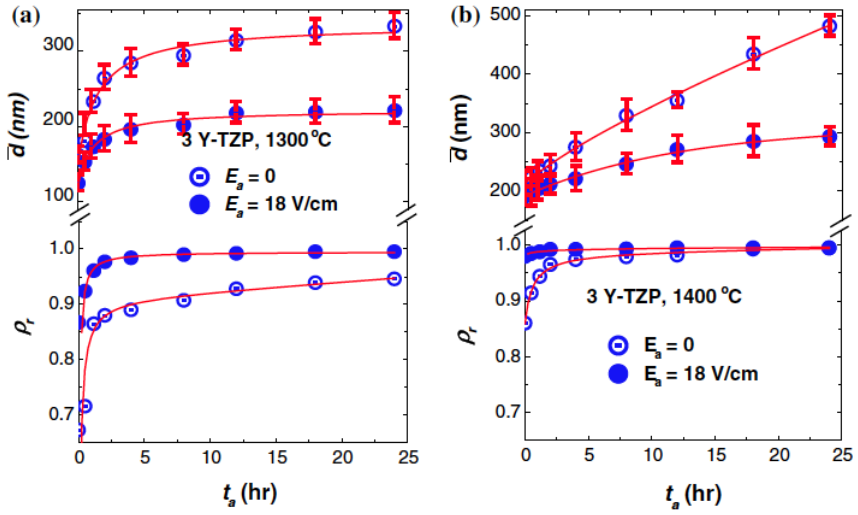

Figure 14: Relative density ρ_r and mean linear intercept grain size d versus annealing time for t_a for the isothermal annealing of 3Y-TZP without and with an applied DC electric field E=18V/Cm (a) at 1300°C and (b) at 1400°C. (Reproduced from [21])

While the resulted microstructure showed retardation in the grain size, it does not necessarily indicate grain growth retardation, due to the combination of several phenomena that occurred in those treatments and their influence on each other. Therefore one should be very careful with conclusions regarding the influence of electric fields on grain growth from this kind of experiment.

2.10 Silicon Carbide in SPS

Frage and Hayun sintered silicon carbide using SPS [4]. While conventional pressure-less sintering of silicon carbide with 15°C/min heating and cooling rates and 1 hour dwell at 2100°C resulted in a maximum ~96% of the theoretical density and an eqiuaxed microstructure [24], SPS resulted in full density (~100%) and an equiaxed microstructure as shown in Figure 15, using heating and cooling rate of 400°C/min and only 0-10 min dwell

at 2050°C under vacuum of 1.3 h Pa and uniaxial pressure of 69 MPa. The short sintering times of silicon carbide in SPS and the full density in comparison with conventional sintering encourages further investigation of the mechanism behind this result, because short sintering time can limit grain growth, and a microstructure with fine grains and full density may show improvement of properties such as strength.

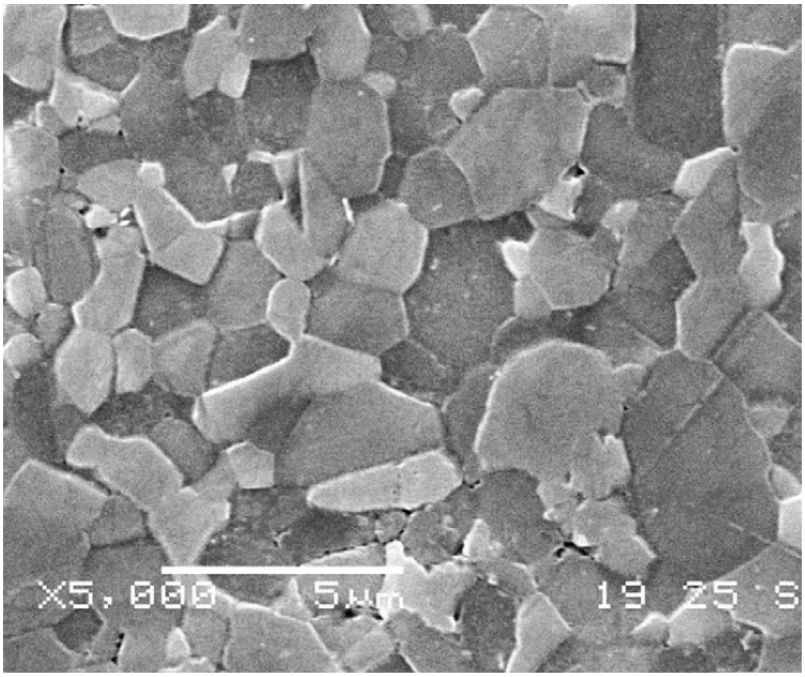

Figure 15: Backscattered electron SEM micrograph of the microstructure of SiC after SPS with heating and cooling rate of 400°C/min and only 0-10 min dwell at 2050°C under vacuum of 1.3 h Pa and uniaxial pressure of 69 MPa (reproduced from [4]).

3 Research Goals

The goal of this research was to investigate the influence of external fields on grain growth and on effective grain boundary mobility (rather than on sintering). Due to the growing interest in SiC for ballistic armor and the possible microstructural improvement of SiC sintered by SPS, SiC was chosen as a model system to investigate the influence of external fields on grain growth and effective grain boundary mobility by:

1. Measuring the effective grain boundary mobility of SiC during conventional at 2100°C;
2. Comparing the effective grain boundary mobility during conventional annealing to that resulting from SPS at 2100°C (and at 1800°C in order to avoid the possible influence of temperature detection deviation in SPS);
3. Investigating the grain shape (aspect ratio) evolution in SiC during conventional and SPS annealing.

4 Experimental Methods

4.1 Sintering

Densification and grain growth are two processes that can influence each other due to both being based on mass transport of the same mass. In order to avoid the influence of densification on grain growth, there is a need for a system that does not experience densification anymore, i.e. a fully dense body.

The possible complicated influence of impurities on the microstructure in general and on grain growth in particular does not allow to work with commercial samples that may contain unmeasured or unreported impurities. This requires powder preparation and sintering a fully dense body from scratch. As such, in this study sintered samples were prepared for subsequent grain growth experiments.

4.1.1 Powder Preparation

The powder used for the sintering was SiC 6H (0.7μm, Electro abrasives LLC, specifications are listed in

Table 1), which was doped with 0.5 wt.% carbon black, 0.5 wt.% phenolic resin and 0.5 wt.% amorphous boron in order to improve the sintering [24].

Table 1: SiC 6H powder (0.7μm, Electro abrasives LLC) used for the first sintering.

Typical chemical analysis		**Typical particle sizing (Horiba)**	
SiC	98.5 wt.% min.	**D90**	1.811 μm
Free C	2 wt.% max.	**D50**	0.748 μm
O	1.1 wt.% max.	**D10**	0.344 μm
N	0.25 wt.% max.		
Si	0.63 et.% max.		
Fe	800 ppm max./ 300 ppm typical		
Ca	200 ppm max./ 10 ppm typical		
Mo	200 ppm max./ 50 ppm typical		
Al	550 ppm max./ 150 ppm typical		
Zr	50 ppm max./ 12 ppm typical		

The starting powder was ball-milled using SiC balls with diameter of 5mm in a media of acetone with volume ratio of 1:1. A deflocculant (KV 9056, Zschimmer & Schwarz) was added into the mixture as well as phenolic resin that performed as a binder. The ball-milling lasted 12 hours in a polyethylene bottle. After ball-milling the solution was dried in a furnace at 60ºC in air for 6 hours, and then ground using a mortar and pestle. The powder was then sieved through a set of decreasing sieve sizes (96μm, 72μm, 50μm, 25 μm).

4.1.2 Green Body Preparation

In order to sinter in pressure-less conditions, there is a need to produce a green body out of the prepared powder. The first step of the green body production was uniaxial pressing under 27.5 MPa in a die with diameter of 50mm and then cold isostatic pressing at 241 MPa. These two stages resulted in a green body of 65% of theoretical density. The green body density was measured using geometry and weight.

4.1.3 Sintering

The green body was sintered at 2100ºC for 1 hour under flowing He (99.999%) to a relative density of 94%, using heating and cooling rates of 15ºC/min. The sintering process resulted in an average grain size of 2.7μm. The density was measured using the Archimedes method [25].

4.1.4 Annealing

In order to determine the effective grain boundary mobility at a certain temperature, there is a need to conduct annealing experiments for different times and then to measure the average grain size as a function of time as described in section 2.7. In order to maintain uniformity, a single sintered sample of SiC was cut into multiple pieces and then each peace went through a different annealing treatment.

4.1.4.1 Conventional Annealing

Conventional annealing was conducted at 2100ºC with heating and cooling rates of 15°C/min for the following times: 1, 2, 4, 6, 8, 12, and 20 hours.

4.1.4.2 SPS Annealing

SPS annealing was conducted at 2100°C with heating and cooling rate of 400°C/min for 16, 32, 60 and 120 minutes, in order to compare with the conventional annealing, and also at 1800°C in order to eliminate the possible influence of temperature measurement error as described in section 2.4.4. The difference of 300°C between the two annealing temperatures was chosen because it was the largest reported temperature difference between the surface of the die and on the sample reported to the date of this research [26].

4.1.5 Furnaces

The conventional furnace was a cold-wall graphite element furnace, using flowing He (99.999%) to reach an oxygen partial pressure (PO_2) of $5x10^{-15}$ atm. SPS was conducted

using a HPD 5 &10 - FCT system at a vacuum of 1.3 hPa and a minimum uniaxial pressure of 2 MPa (to ensure contact of the sample with the graphite rams).

4.2 Sample Preparation for Characterization

For measurement of the grain size, annealed samples were sectioned and mechanically polished with a diamond slurry down to a particle size of 0.25 µm, and then thermally etched in flowing He (99.999%) at 1800ºC for 20 min using a heating rate of 15ºC/min

4.3 Characterization

Micrographs were acquired using scanning electron microscopy (SEM) using a Zeiss Ultra-Plus FEG-SEM.

4.4 Grain Size Measurements

The grain size was determined from the micrographs using Image-J software and the linear intercept approach. A correction factor of 1.126 was used in order to correlate between the grain size and the measured length [27]:

$$\bar{G} = 1.126\bar{L} \tag{7}$$

The standard error of the mean was calculated with:

$$s.e.m = \frac{s}{\sqrt{N}} \tag{8}$$

where s is the standard deviation of the average and N is the total number of measurements.

4.5 Effective Grain Boundary Mobility

The effective grain boundary mobility was determined by plotting the average grain size as a function of annealing time with linear and parabolic fit as described in section 2.7.

5 Results

5.1 SiC Microstructure after Convectional Sintering at 2100ºC

The microstructure of the sintered (pre-annealed) SiC is presented in Figure 16, showing approximately equi-axed grains, and residual pores mostly located at grain boundaries and triple junctions. The density was determined using the Archimedes method resulting in 94% ± 0.3 of the theoretical density, and an average grain size of 2.36±0.06 µm.

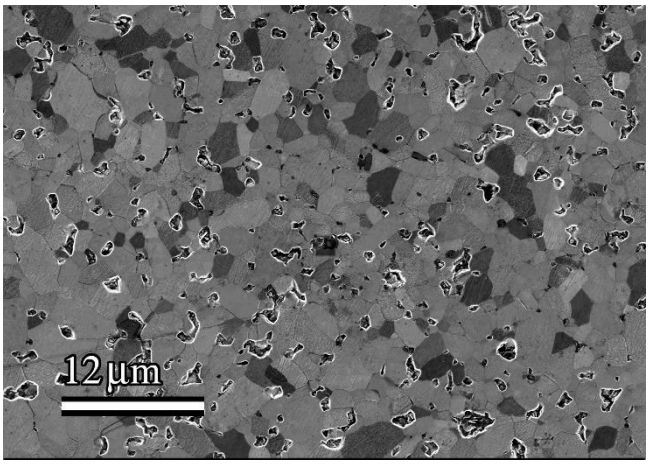

Figure 16 Backscattered electron SEM micrograph of the microstructure of SiC after sintering.

5.2 SiC Microstructure after Convectional Annealing at 2100ºC

The microstructure of the sample conventionally annealed for 4 hours at 2100ºC is presented in Figure 17, showing moderate grain growth and slightly elongated grains. The average grain size was determined to be 3.06±0.09 µm. A histogram of the grain size distribution is presented in Figure 18, showing single-mode distribution.

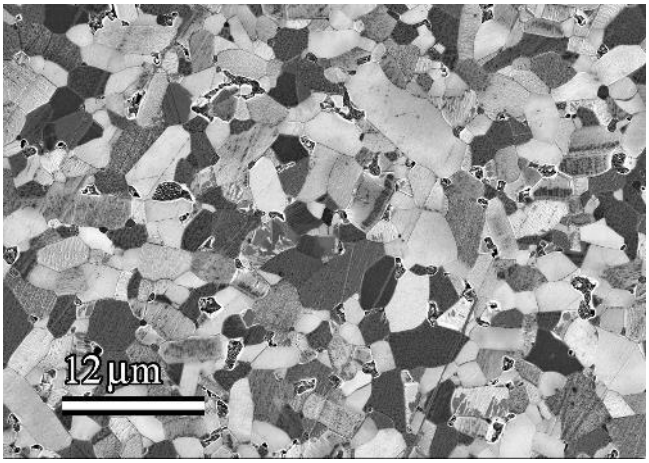

Figure 17 Backscattered electron SEM micrograph of the SiC microstructure after 4 hours conventional annealing at 2100ºC.

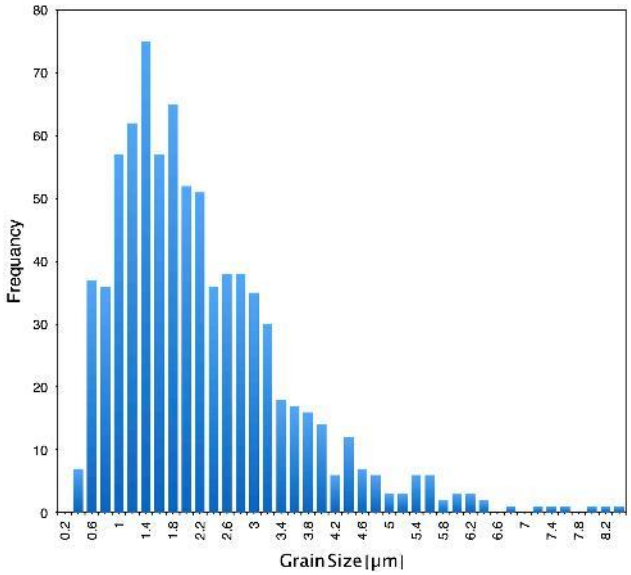

Figure 18: SiC grain size distribution after 4 hours of conventional annealing at 2100ºC.

5.3 Effective Grain Boundary Mobility under Conventional Annealing

The effective grain boundary mobility of SiC which was conventionally annealed at 2100ºC was determined by plotting the average grain size squared as a function of time as shown in Figure 19, resulting in an effective mobility of $3.53 \pm 0.08 \cdot 10^{-17}$ m^2/sec. It can be seen that a parabolic fit shows a relatively strong match with $R^2=0.9952$, as expected for normal grain growth.

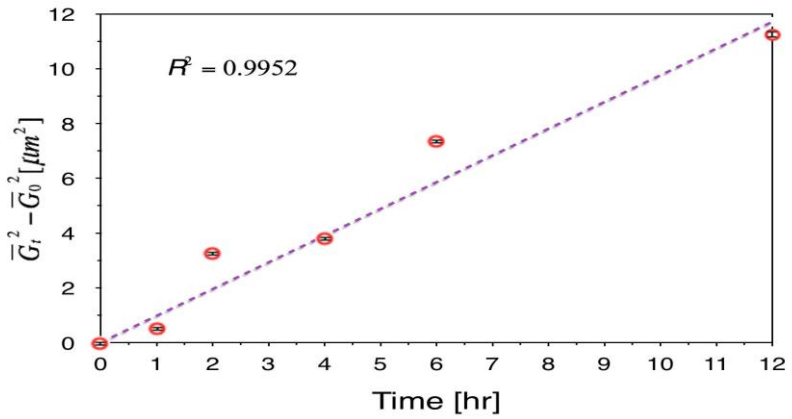

Figure 19: Grain growth kinetics of SiC conventionally annealed at 2100ºC.

Table 2: Raw data of Figure 19.

Time [hr]	Average Grain Size [µm]	Standard Deviation [µm]	Standard Error of the Mean [µm]
0	2.36	1.58	0.06
1	2.46	1.85	0.07
2	2.97	2.11	0.08
4	3.06	2.38	0.09
6	3.6	2.93	0.1
12	4.1	3.8	0.17

5.4 SiC Microstructure after SPS Annealing At 2100ºC

The microstructure of a SiC sample annealed for 16 min by SPS at 2100ºC is presented in Figure 20, showing significant grain growth after only 16 minutes, slightly elongated grains, and occluded pores unlike in the pre-annealed sample or in the conventionally annealed sample. A histogram of the grain size distribution of this sample is presented in Figure 21, indicating also a single-mode distribution.

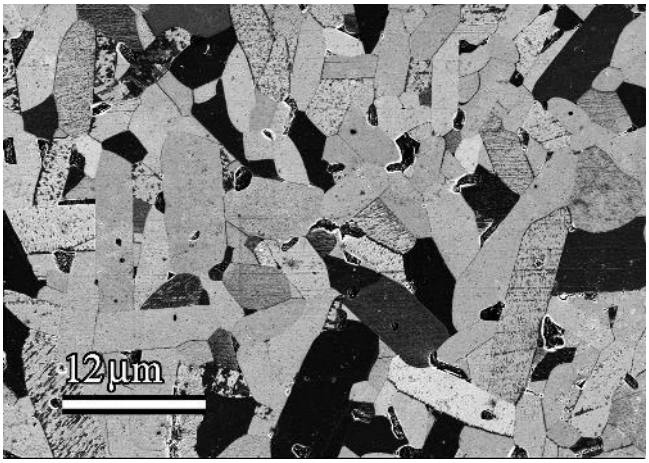

Figure 20: Backscattered electron SEM micrograph of SiC after 16 min of annealing at 2100ºC using SPS.

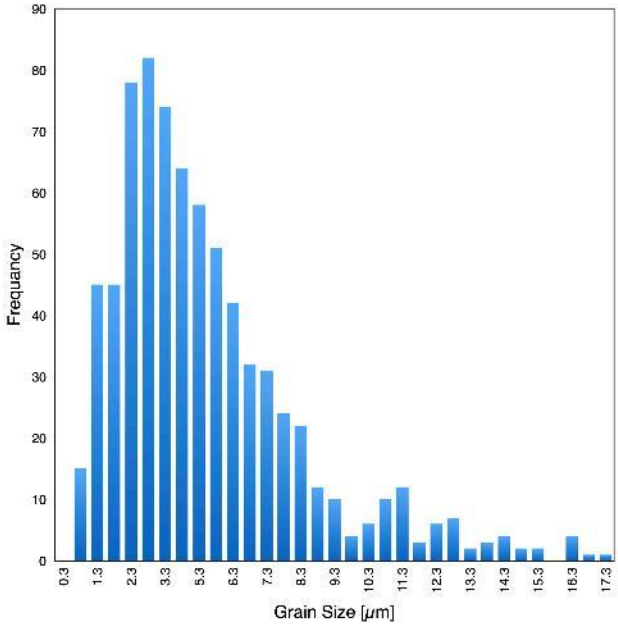

Figure 21: SiC grain size distribution after 16 min of annealing at 2100ºC using SPS.

The microstructure of the SiC sample annealed by SPS for 32 min at 2100ºC is presented in Figure 22, showing a diverse population, exaggerated grain growth, extremely elongated grains, a significant amount of occluded pores, and penetration of anisotropic small grains into larger grains. Most of the grains shown here, after 32 min of annealing by SPS, are larger than those after conventional annealing after 4 hours, indicating different grain growth kinetics or a different grain growth mechanism.

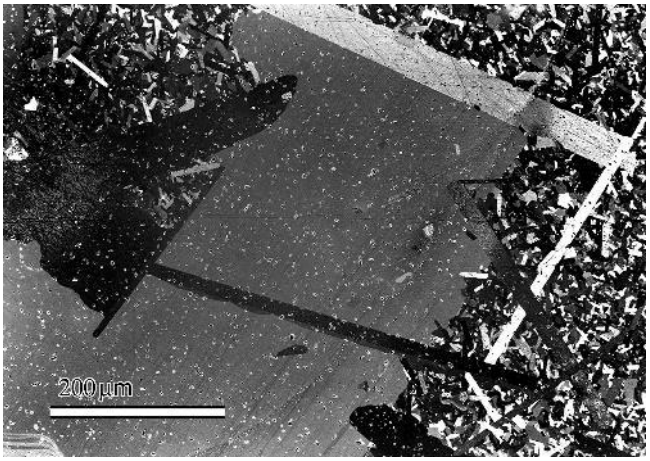

Figure 22: Backscattered electron SEM micrographs of SiC after 32 min of annealing using SPS at 2100ºC.

The microstructure of the sample annealed for 120 min by SPS at 2100ºC is presented in Figure 23, showing a larger magnitude of the same phenomena seen in the sample annealed by SPS for 32 min.

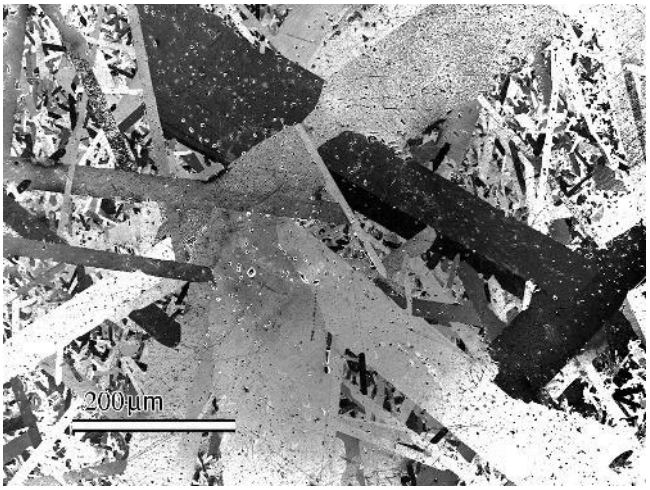

Figure 23: Backscattered electron SEM micrograph of SiC microstructure after 120 min of annealing using SPS at 2100ºC.

5.5 Effective Grain Boundary Mobility under SPS Annealing at 2100ºC

Since the parabolic fit approach that was used to determine the effective grain boundary mobility of SiC in conventional annealing had a relatively low R^2 (0.9159) when it was used to determine the effective grain boundary mobility of SiC in SPS annealing, there was a

need for different approaches of analysis to obtain a higher confidence in the different mobility numbers for SPS in comparison with conventional annealing, including calculation of mobility for the relatively small population of grains from the notion that the exaggerated grains might have different grain growth mechanism in comparison with the small grains. Figure 24 presents four different approaches used to determine the effective grain boundary mobility of SiC annealed by SPS at 2100ºC; using a parabolic fit of the entire grain population resulting in an effective grain boundary mobility of $4.79\pm0.01\cdot10^{-14}$ m^2/sec; a linear fit of the entire grain population resulting in an effective grain boundary mobility of $1.5\pm0.08\cdot10^{-14}$ m^2/sec, a parabolic fit of the small grains resulting in an effective grain boundary mobility of $3.86\pm0.01\cdot10^{-14}$ m^2/sec, and a linear fit of the small grains resulting in an effective grain boundary mobility of $1.36\pm0.09\cdot10^{-14}$ m^2/sec. All four analysis methods result in values for the effective grain boundary mobility which are 3 orders of magnitude ***larger*** than the effective grain boundary mobility resulting from conventional annealing. The linear fit had a larger R^2 in comparison with the parabolic fit, as expected for abnormal grain growth, and the separate analysis for small grain population and for the entire population didn't show a significant difference, which can't prove the presence of different mechanism of grain growth for the large grains rather than in small grains.

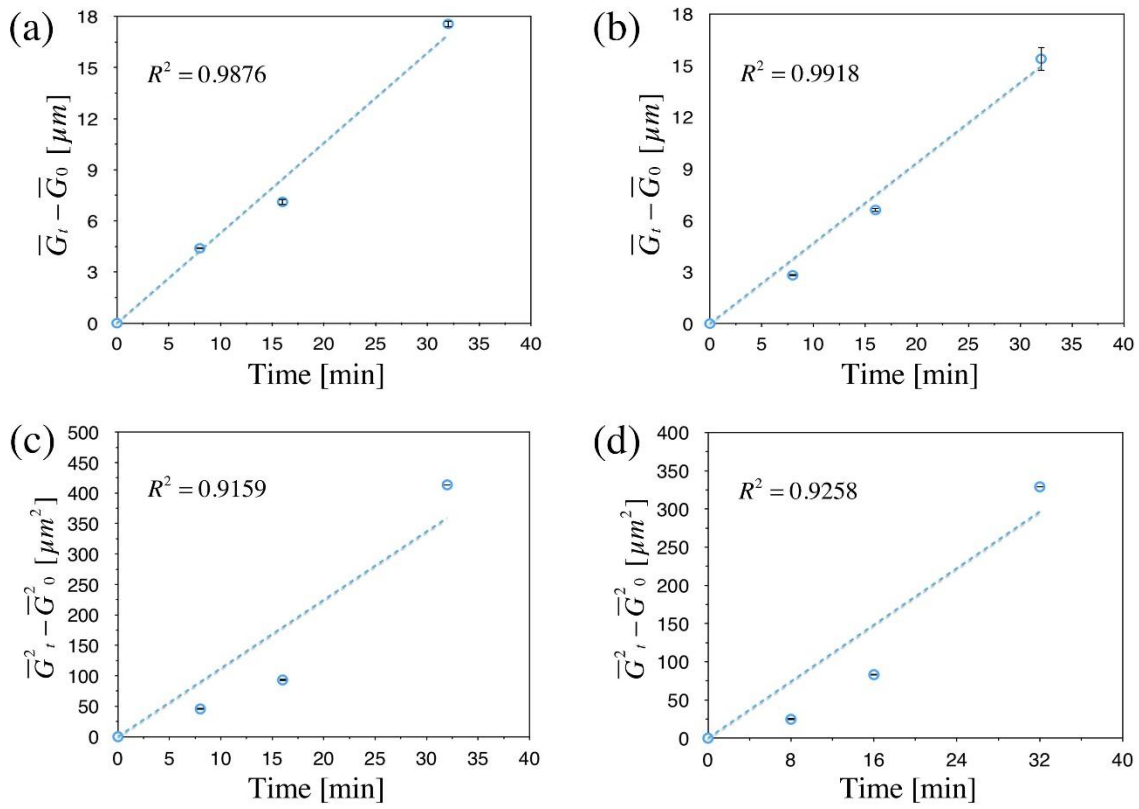

Figure 24: Grain growth kinetics of SiC in SPS at 2100ºC using (a) a linear fit to the entire population of grain sizes; (b) a linear fit to small grains only; (c) a parabolic fit to the entire grain size population; and (d) a parabolic fit to the small grains.

Table 3: Raw data of Figure 24 (a) and (c).

Time [min]	Average Grain Size of Entire Population [µm]	Standard Deviation [µm]	Standard Error of the Mean [µm]
0	2.36	1.58	0.06
8	6.93	3.79	0.12
16	9.71	7.67	0.29
32	20.24	11.03	0.39

Table 4: Raw data of Figure 24 (b) and (d).

Time [min]	Average Grain Size of Small Grains Only [µm]	Standard Deviation [µm]	Standard Error of the Mean [µm]
0	2.36	1.58	0.06
8	5.28	2.26	0.08
16	9.24	2.82	0.1
32	18.08	3.67	0.13

5.6 SiC Microstructure after SPS Annealing At 1800ºC

The microstructure of SiC annealed by SPS for 16 min at 1800ºC is presented in Figure 25, showing moderate grain growth, approximately equi-axed grains, and pores located mainly at grain boundaries and triple junctions, like in the pre-annealed sample and after conventional annealing and unlike in the samples annealed in SPS at 2100°C. The average grain size was determined to be 2.42±0.06 µm.

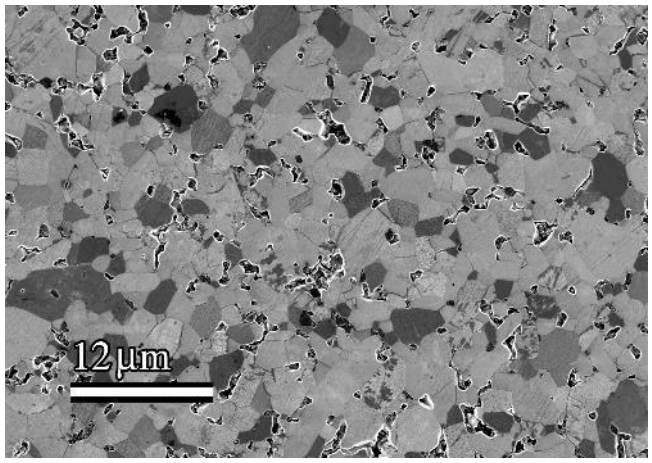

Figure 25: Backscattered electron SEM micrograph of SiC microstructure after 16 min of SPS annealing at 1800ºC

The effective grain boundary mobility of SiC annealed by SPS at 1800ºC was determined by plotting the squared average grain size as a function of time as shown in Figure 26, resulting in $6.2 \pm 0.11 \cdot 10^{-17}$ m^2/sec with $R^2=0.9952$.

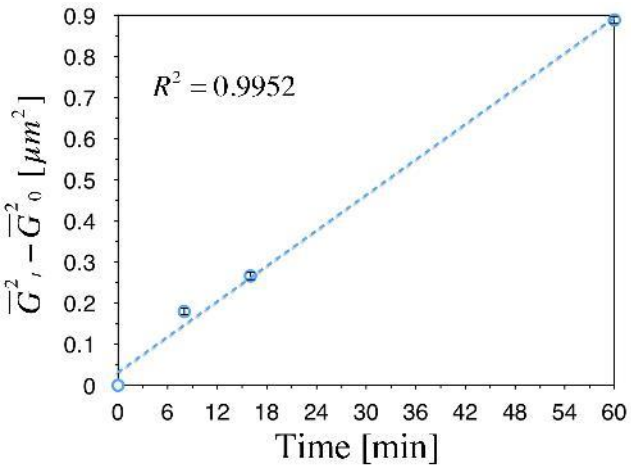

Figure 26 Grain growth kinetics of SiC in SPS at 1800ºC.

Table 5: Raw data of Figure 26.

Time [min]	Average Grain Size [µm]	Standard Deviation [µm]	Standard Error of the Mean [µm]
0	2.36	0.96	0.03
8	2.40	1.21	0.05
16	2.42	1.47	0.06
32	3.54	2.20	0.09

The different effective grain boundary mobilities are summarized in

Table 6.

Table 6 Effective grain boundary mobility of SiC annealed by conventional furnace and SPS.

2100°C Conventional All Population - Parabolic	2100°C SPS All population – Parabolic	2100°C SPS Small population - Parabolic	2100°C SPS All population – Linear	2100°C SPS Small population - Linear	1800°C SPS All population - Parabolic
$3.53 \cdot 10^{-17}$ [m^2/sec]	$4.79 \cdot 10^{-14}$ [m^2/sec]	$3.86 \cdot 10^{-14}$ [m^2/sec]	$1.54 \cdot 10^{-14}$ [m^2/sec]	$1.36 \cdot 10^{-14}$ [m^2/sec]	$6.22 \cdot 10^{-17}$ [m^2/sec]

5.7 Aspect Ratio as a Function of Annealing Time

Examination of the microstructure evolution during SPS annealing shows that the grains become more elongated as a function time. In order to quantify the elongation of the grains, a distribution of the grain aspect ratio as a function of SPS annealing time at 2100ºC was plotted. The distributions are presented in Figure 27, showing an increase of the aspect ratio as a function of time and a broadening of the distribution, i.e. increasing diversity in the population as a function of SPS annealing time.

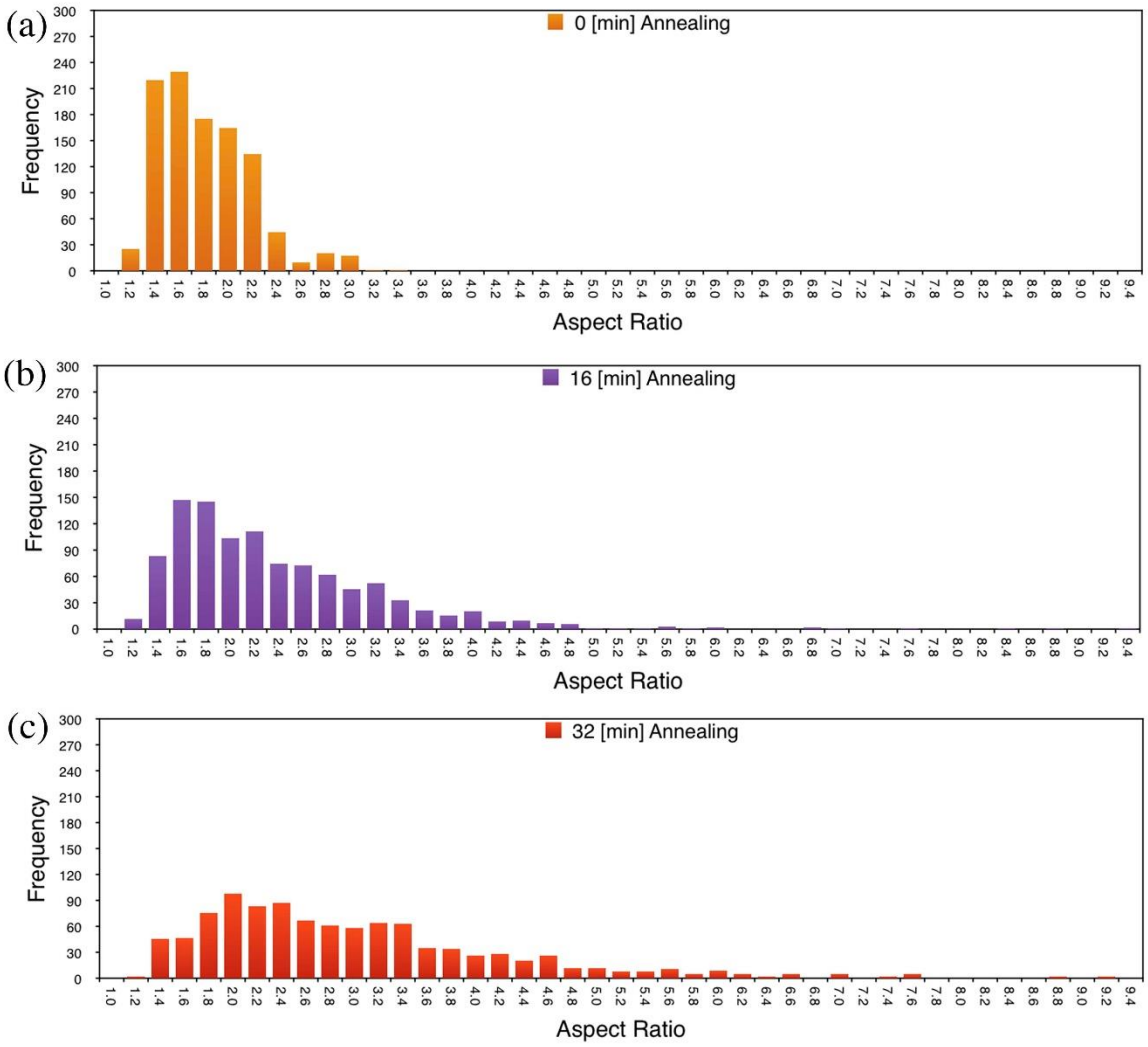

Figure 27: Grain aspect ratio as a function of annealing time in SPS at 2100ºC for (a) 0 min annealing (b) 16 min annealing and (c) 32 min annealing.

In order to understand whether the increase in the aspect ratio as a function of time is a unique phenomenon for grain growth in SPS or a general phenomenon in SiC, the aspect ratio as a function of annealing time during conventional annealing was calculated as well. The aspect ratio as a function of time for both conventional and SPS annealing is presented in Figure 28, showing different trends, where the aspect ratio as a function of time increases much faster during SPS annealing compared to conventional annealing.

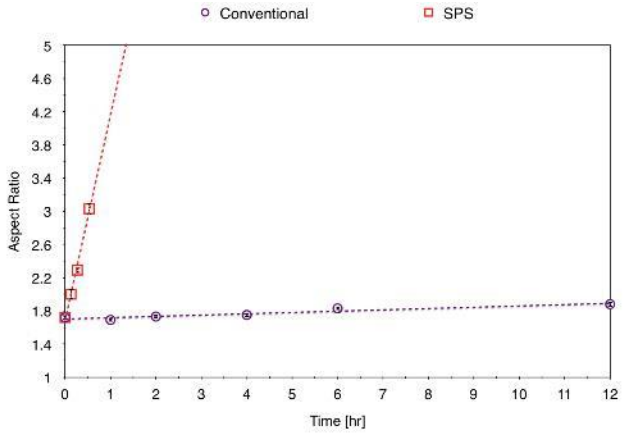

Figure 28: Aspect ratio as a function of annealing time for conventional and SPS annealing at 2100ºC.

Table 7: Raw data of Figure 28.

Conventional Annealing			
Time [hr]	Aspect Ratio	Standard Deviation	Standard Error of the Mean
0	1.64	1.12	0.04
1	1.69	0.96	0.04
2	1.73	1.15	0.05
4	1.75	1.1	0.05
6	1.82	1.15	0.05
12	1.87	1.29	0.06
SPS Annealing			
Time [min]	Aspect Ratio	Standard Deviation	Standard Error of the Mean
8	2.14	1.42	0.06
16	2.29	1.45	0.06
32	3.02	3.38	0.14

5.8 Aspect Ratio as a Function of Grain Size

Although the increase in the aspect ratio as a function of time during SPS is significantly larger than during conventional annealing and it might indicate preferred growth directions in SPS, the grain size after SPS annealing was significantly larger as well, in compression with the grain size after conventional annealing, and the reason for the increase in the aspect ratio during SPS annealing may lay within the large grain size and not a preferred growth orientation in SPS. The aspect ratio as a function of grain size for conventional and SPS annealing is presented in Figure 29, showing the same trend for both annealing methods, unlike in the graph of aspect ratio as a function of time.

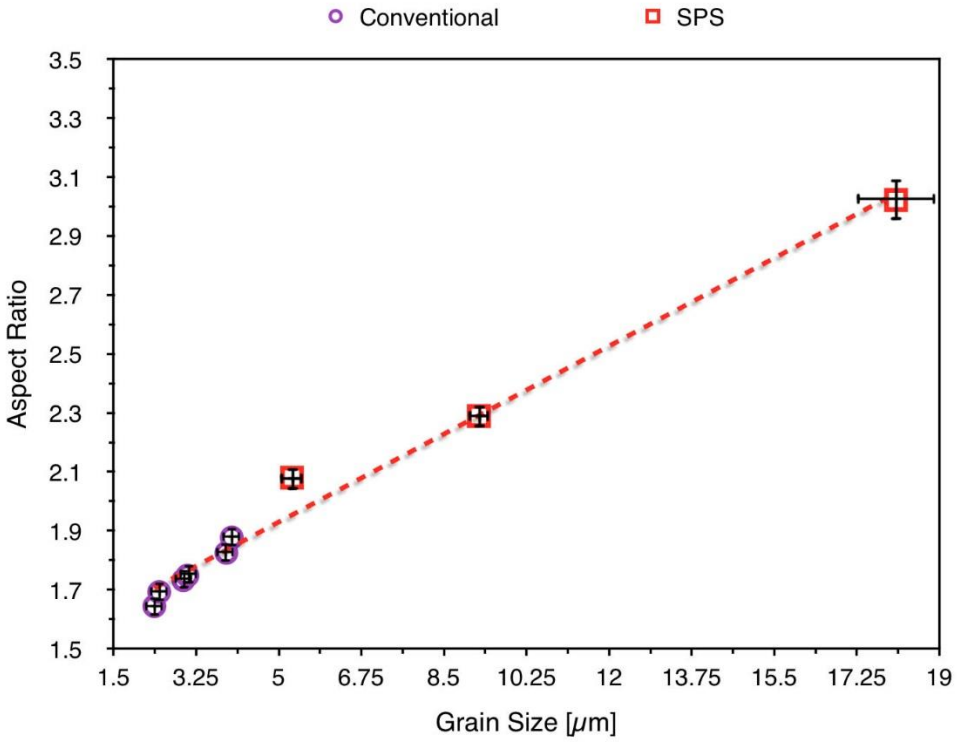

Figure 29: Aspect ratio as a function of grain size in conventional and SPS annealing at 2100ºC.

Table 8: Raw data for Figure 29.(for standard deviation and Standard error pf the mean see Table 2 and Table 7)

Conventional Annealing	
Average Grain Size [µm]	Aspect Ratio
2.36	1.64
2.46	1.69
2.97	1.73
3.06	1.75
3.89	1.82
4.01	1.87
SPS Annealing	
Average Grain Size [µm]	Aspect Ratio
5.28	2.14
9.24	2.29
18.08	3.02

5.9 Grain Growth Orientation as a Function of Electrical Field Direction

Given the large aspect ratio of the exaggerated grains resulting from extended SPS annealing, additional samples were investigated as a function of the direction of the applied electric field. The microstructure of the sample annealed by SPS parallel and perpendicular to the electric field is presented in Figure 30, showing no correlation between the electric field direction and the grain orientation.

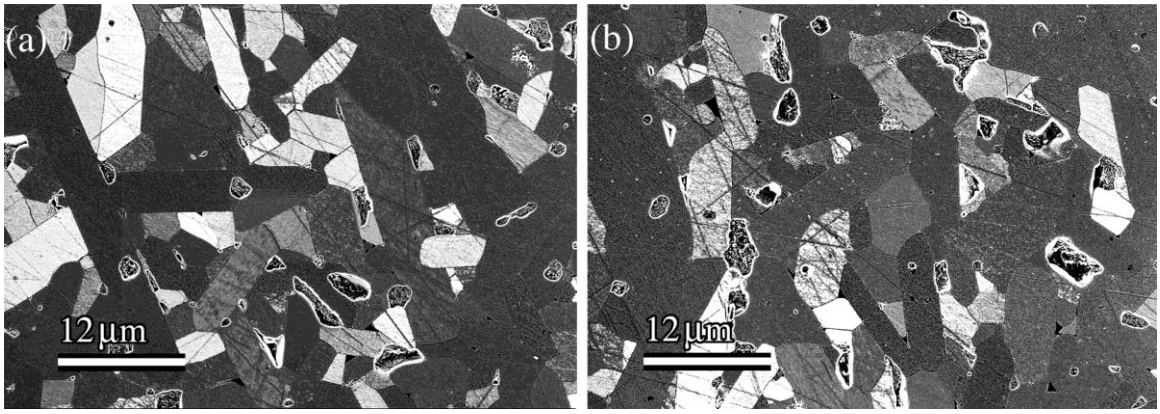

Figure 30: Backscattered electron SEM micrographs of SiC microstructure (a) perpendicular to the electrical field and (b) parallel to the electrical field.

6 Discussion

6.1 The Effective Grain Boundary Mobility of SiC in Conventional and SPS Annealing

The effective grain boundary mobility of SiC annealed by SPS was 3 orders of magnitude larger than that for conventional annealing at 2100ºC in all four different approaches of analysis. The measured grain boundary mobility of SiC annealed by SPS at 1800ºC was twice as large as that of conventional annealing at 2100ºC, and annealing by SPS at 2100ºC resulted in significant grain growth, and exaggerated elongated grains, unlike in conventional annealing or in SPS annealing at 2100°C. These facts might point to a different mechanism for grain boundary migration during SPS annealing at 2100°C.

A possible reason for the difference in the microstructural evolution between the two annealing methods may reside within the difference in the heating technique. While heating for conventional annealing is by convection from the surface (which is heated by radiation and convection), in SPS heating results in part from the electrical current that is flowing through the surrounding die *and* the sample. The sample is placed electrically parallel to the die, and while most of the current flows through the die, that is made of graphite and has a low electrical resistance of 30-600 [μΩ·m] [28], some of the current flows through the sample as that has a higher electrical resistance of $3\text{-}1 \cdot 10^{-4}$ [Ω·m] [29].

The relatively small flux of current that flows through the sample would mostly follow paths of least resistance. The current generates Joule heating along its paths, and this Joule heating can affect the grain boundary mobility in various ways. Joule heating of the grain boundary

can increase grain boundary diffusion, or with enough energy can create complexion transitions which may enhance the grain boundary mobility [30,31].

The phenomena that occurred during microstructural evolution in SPS annealing at 2100°C (exaggerated growth) and that were absence in SPS annealing at 1800°C, may indicate a critical on-set point, in a certain temperature, that might ignite secondary mechanism(s) aside from the already working mechanisms that exist in microstructural evolution during conventional annealing. Further investigation of more points at different temperatures between 1800°C and 2100°C may shed light on the existence of an on-set point.

6.2 The Influence of Electrical Field on Grain Growth

In addition to the presence of an electrical current and its possible influence on microstructural evolution, an electrical field is present in the system as well. As explained in section 2.9, studies on the influence of electrical fields on grain growth claimed that electrical fields retard grain growth, or in other words reduce the mobility.

In this study we clearly show that SPS annealing, where an electric field is almost constantly present, significantly enhances (3 orders of magnitude) the mobility. This is in contradiction with the interpretation of the results that was reported in the literature [21, 22, 23].

While the studies in the literature show a microstructure with smaller grain size in the presence of electric fields, and from that concluding that electrical fields retard grain growth, the problem with these reports is that the measurement of grain growth was mixed with sintering. During sintering other processes in addition to grain growth occur, such as densification, that may affect grain growth, and as such previous conclusions regarding the influence of electrical fields on grain growth were inadequately founded.

Though in this study there is no doubt regarding the enhancement of grain growth during SPS annealing of SiC, i.e. mobility enhancement in the presence of electric field, one should not promptly expect the same behavior with the materials studied in the literature (YSZ for example). One should take into account that SiC (semiconductor) and YSZ (dielectric insulator) may interact differently with the electric field during sintering. From the difference or the similarity of the grain growth regime of YSZ in comparison with SiC when repeating the same method of the experiments in this study, one may conclude on the manner and the intensity of the electric field influence on grain growth.

6.3 The Influence of Electrical Field on Grain Orientation

If the presence of the electrical field in SPS does influence grain growth we may expect to see a correlation between the grain orientation and the applied electrical field after annealing by SPS. However, this concept is not corroborated by our results, which show no correlation between the electrical field direction and the orientation of grain growth (Figure 30 section 5.9). It does not mean though that because that the electrical field has specific orientation it will necessarily affect the microstructure evolution anisotropically, so it does not revoke an influence of the electrical field.

6.4 Anisotropy

6.4.1 Possible Reasons for Anisotropy

The microstructural evolution during SPS annealing shows increasing anisotropy as a function of time, which evolves much faster than in conventional annealing. A grain shape that is changing as a function of time means that some of the grain boundaries need to

accelerate as a function of time as demonstrated in Figure 31 and Figure 32. This may indicate that the system does not reach steady state, i.e. SPS causes either a change in mechanism or an anisotropic change in mobility preventing steady-state growth.

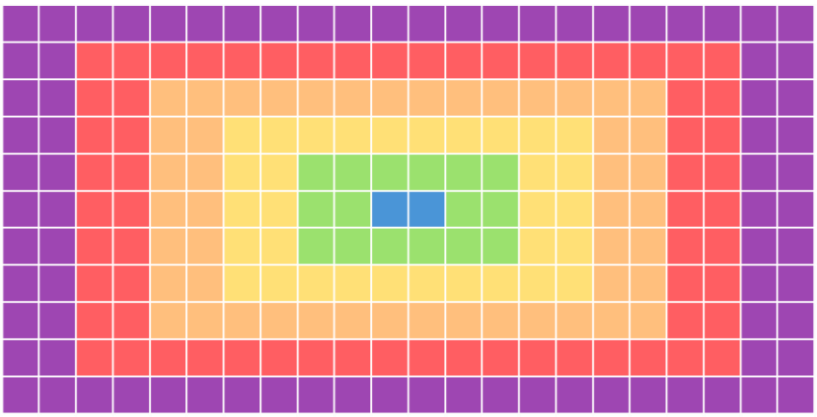

Figure 31: Schematic illustration of constant aspect ratio as a function of time; constant velocity of grain boundaries, with different velocities for each boundary.

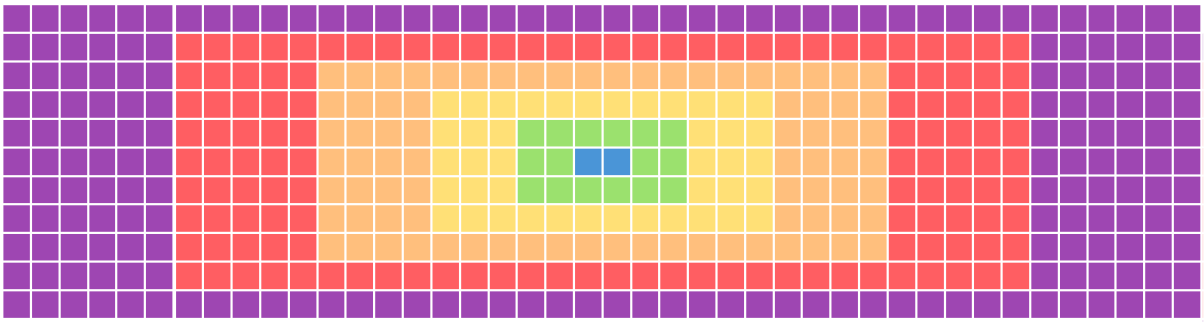

Figure 32: Schematic illustration of changing aspect ratio as a function of time; acceleration (different accelerations) of grain boundaries.

6.4.2 Possible Extrapolation of the Aspect Ratio as a Function of Grain Size

Although the aspect ratio as a function of annealing time (Figure 28) shows a much larger slope for SPS annealing, and that may lead to a thought that SPS influence enhanced anisotropy, the grain size after SPS annealing was much larger as well, and the reason for the anisotropy may lie within the enormous grain size, i.e. this phenomenon could be a natural phenomenon of SiC and it can be only clearly observed for large values of grain size.

The aspect ratio as a function of grain size (Figure 29) shows that the aspect ratio evolution in conventional annealing and in SPS follow the same function, i.e. as for SPS, the aspect ratio during conventional annealing also does not reach steady-state. A more reasonable behavior would be that the actual continuity of the graph for conventional annealing would not keep the same trend and at some point would flatten-out as demonstrated in Figure 33, resulting in a constant aspect ratio, and perhaps SPS would follow the same trend, as it may be concluded from the enormous grain that can be seen in Figure 23.

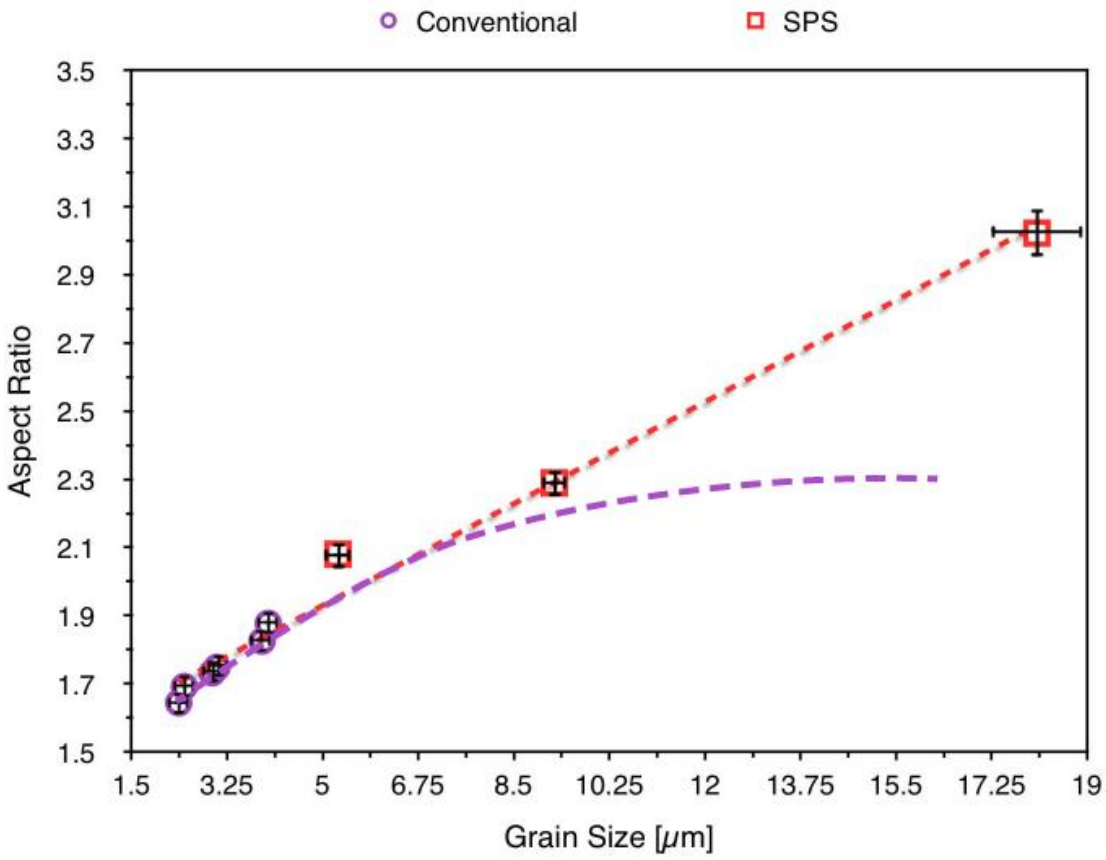

Figure 33: Schematic illustration of possible extrapolation of the graph of aspect ratio as a function of grain size in conventional and SPS annealing.

7 Summary and Conclusions

This study used SiC as a model system in order to explore to influence of electrical fields on grain growth. To the best of our knowledge, this is the first time that an electric field was demonstrated to accelerate grain growth.

The effective grain boundary mobility of SiC conventionally annealed at 2100°C was determined to be $3.53\pm0.076\cdot10^{-17}$ m^2/sec. The effective grain boundary mobility of SiC annealed by SPS at 2100ºC was 1.36-4.39·10^{-14} m^2/sec depending on the method of analysis, and the effective grain boundary mobility of SiC annealed by SPS at 1800ºC was $6.22\cdot10^{-17}$ m^2/sec, i.e. the grain boundary mobility of SiC annealed by SPS was 3 orders of magnitude larger than that achieved by conventional annealing at 2100°C and twice as large at 1800ºC in SPS rather than in conventional annealing.

The direction of the applied electric field in SPS showed no correlation with the orientations of the grains after the annealing. The grain aspect ratio from conventional annealing and from SPS annealing showed a different dependence in time and the same dependence on grain size. This may lead to the conclusion that the crystal shape does not reach steady state when using SPS.

The microstructure evolved by SPS annealing compared to that by conventional annealing shows that SPS results in a different grain growth mechanism(s) than during conventional heating, but the applied electric field does not affect the direction of anisotropic grain growth.

The significant difference in the effective grain boundary mobility and microstructure is probably due to Joule heating at grain boundaries.

8 Recommendations for Future Work

To the best of our knowledge, this is the first time that the influence of an electric field was demonstrated to accelerate grain growth. This demands farther exploration in order to understand whether it is a unique case for SiC, a unique case for SPS, or a general phenomenon. There is also a need to separately explore the influence of the current and electric field. This requires expansion of this work to materials other than SiC, including ionic materials.

Another important parameter that my influence the observed phenomena is the high heating and cooling rates in SPS (400°C/min) in comparison with conventional annealing (15°C/min), so expanding this work to different heating rates in SPS may confirm/reject this hypothesis.

In order to shed light on the mechanism(s) that lead to exaggerated grain growth, the grain boundary structure and chemistry of the elongated and equiaxed grains should be characterized after SPS/flash/conventional annealing. Another parameter that should be explored is the grain boundary mobility as a function of temperature for conventional and SPS annealing. Lastly, the contribution of electrical energy to the system on the absolute temperature may also to help understand the observed phenomena.

1. References

1. Anderson Jr CE, Behner T, Holmquist TJ and Orphal DL. *Penetration response of silicon carbide as a function of impact velocity*, International Journal of Impact Engineering **38**, 892-899. 2011.
2. Munir, Z. a., Anselmi-Tamburini, U. & Ohyanagi, M. *The effect of electric field and pressure on the synthesis and consolidation of materials: A review of the spark plasma sintering method,* J. Mater. Sci. **41,** 763–777, 2006.
3. Guillard, F., Allemand, A., Lulewicz, J.-D. & Galy, J. *Densification of SiC by SPS-effects of time, temperature and pressure*, J. Eur. Ceram. Soc. **27,** 2725–2728, 2007.
4. Hayun, S., Paris, V., Mitrani, R., Kalabukhov, S., Dariel, M. P., Zaretsky, E., & Frage, N. *Microstructure and mechanical properties of silicon carbide processed by Spark Plasma Sintering (SPS),* Ceramics International, **38**[8], 6335–6340, 2012.
5. Conrad, H. & Wang, J. *Equivalence of AC and DC electric field on retarding grain growth in yttria-stabilized zirconia,* Scr. Mater. 72-73, 33–34, 2014.
6. Narayan, J. *Grain growth model for electric field-assisted processing and flash sintering of material,* Scr. Mater. **68**, 785–788 ,2013.
7. Powers, J. D. & Glaeser, A. M. *Grain Boundary Migration in Ceramics,* Interface Sci. **39**, 23–39 ,1998.
8. S.-J. L. Lang, *Sintering - Densification, Grain Growth, and Microstructure,* Elsevier Butterworth Heinemann, Oxford, UK, 2005.
9. Dillon, S. J., & Harmer, M. P. *Relating grain-boundary complexion to grain-boundary kinetics II: Silica-doped alumina*, Journal of the American Ceramic Society, **91**(7), 2314–2320, 2008.

10. J. A. Lewis, *Colloidal Processing of Ceramics,* Journal of the American Ceramic Society, **83**[10]:2341-2359, 2000.

11. .L. L. Snead, T. Nozawa, Y. Katoh, T.-S. Byun, S. Kondo, D. A. Petti, *Handbook of SiC properties for fuel performance modeling*, Journal of Nuclear Materials, **371**[1–3]:329-377, 2007

12. W. Y. Ching, Y.-N. Xu, P. Rulis, L. Ouyang, The electronic structure and spectroscopic properties of 3C, 2H, 4H, 6H, 15R and 21R polymorphs of SiC, Materials Science and Engineering: A, 422[1–2]:147-156, 2006.

13 P. Shaffer, A review of the structure of silicon carbide, Acta Crystallographica Section B, 25[3]:477-488, 1969.

14. Munir, Z. a., Anselmi-Tamburini, U., & Ohyanagi, M. *The effect of electric field and pressure on the synthesis and consolidation of materials: A review of the spark plasma sintering method,* Journal of Materials Science, **41**[3], 763–777, 2006

15. J. E. Garay, *Current-Activated, Pressure-Assisted Densification of Materials*, Annu. Rev. Mater. Res. **40**[1], 445–468, 2010.

16. R. Orrù, R. Licheri, A. M. Locci, A. Cincotti, and G. Cao, *Consolidation/synthesis of materials by electric current activated/assisted sintering*, Mater. Sci. Eng. R Reports, **63**[4–6], 127–287, 2009.

17. Anselmi-Tamburini, U., Gennari, S., Garay, J. E. & Munir, Z. a. *Fundamental investigations on the spark plasma sintering/synthesis process*, Mater. Sci. Eng. A **394**, 139–148, 2005.

18. H. Gleiter, *The mechanism of grain boundary migration*, Acta Metall., **17**[5] 565-573, 1969.

19. H. Gleiter, *Theory of grain boundary migration rate*, Acta Metall., **17**[7] 853-862, 1969.

20. M. Hillert, *On the theory of normal and abnormal grain growth*, Acta Metall., **13**[3] 227-238, 1965.

21. Wang, J. & Conrad, H. *Contribution of the space charge to the grain boundary energy in yttria-stabilized zirconia,* J. Mater. Sci. **49**, 6074–6080, 2014.

22. Conrad, H., & Wang, J. *Equivalence of AC and DC electric field on retarding grain growth in yttria-stabilized zirconia,* Scripta Materialia, *72-73*, 33–34, 2014.

23. Narayan, J. *Grain growth model for electric field-assisted processing and flash sintering of materials*, Scripta Materialia, **68**[10], 785–788, 2013.

24. E. Gross, D.B. Dahan & W.D. Kaplan, *The role of carbon and SiO2 in solid-state sintering of SiC*, Journal of the European Ceramic Society, **35**[7]:2001-2005, 2015.

25. http://www.csudh.edu/oliver/satcoll/archmede.htm

26. Y. Wang, *Study of temperature field in spark plasma sintering*, Materials Science and engineering: B **90**[1-2], 34-37, 2002.

27. M. I. Mendelson, *Average Grain Size in Polycrystalline Ceramics*, Journal of the American Ceramic Society, **52**[8]:443-446, 1969.

28. http://hyperphysics.phy-astr.gsu.edu/hbase/tables/rstiv.html

29. R. Shinavski, Y. Katoh and L. Snead, Mechanical, *Thermal and Electrical Properties of Nuclear-Grade Silicon Carbide Composites.*

30. W.D. Kaplan, D. Chatain, P. Wynblatt & W.C. Carter, *A Review of Wetting Versus Adsorption, Complexions, and Related Phenomena: The Rosetta Stone of Wetting*, Journal of Materials Science, **48**[17]:5681-5717, 2013.

31. R. Akiva, A. Katsman & W.D. Kaplan, *Anisotropic Grain Boundary Mobility in Undoped and Doped Alumina*, Journal of the American Ceramic Society, **97**[5]:1610-1618, 2014.

השפעה של שדות חשמליים על גידול גרעינים בצורן פחמני

אמיר גבאי

השפעה של שדות חשמליים על גידול גרעינים בצורן פחמני

חיבור על מחקר

לשם מילוי חלקי של הדרישות לקבלת התואר
מגיסטר למדעים במדע והנדסה של חומרים

אמיר גבאי

הוגש לסנט הטכניון - מכון טכנולוגי לישראל

ניסן התשע"ה **חיפה** **אפריל 2015**

תודות

מחקר זה נערך בהנחיית פרופ' וויין ד. קפלן מהפקולטה למדע והנדסה של חומרים בטכניון - מכון טכנולוגי לישראל.
אני מודה לטכניון על התמיכה הכספית הנדיבה בהשתלמותי.

ברצוני להוקיר תודה למנחה שלי פרופ' וויין ד. קפלן על ההדרכה והעידוד לאורך המחקר, על האמונה בדרכי, על לימוד הדרך לביצוע מחקר ועל הכרת העולם המדעי בכלל.

אני רוצה להודות לחברי קבוצת המחקר על העזרה והתמיכה לאורך כל הדרך: הדס שטרנליכט, ערן גרוס, רות משה, גלית עטיה, רן עקיבא, דנה בנס, הדר (בראט) נהור, אורן שני ותומר שטיין.

תודה מיוחדת לאורי וינברג ורחל מארדר על העזרה במחקר.

לסיום ברצוני להודות לפרופ' נחום פרגה ודוקטור שמואל חיון על העזרה בביצוע הניסויים במערכת ה**SPS**.

תקציר

סנטור הוא תהליך שבו אבקה או גוף ירוק הופכים לגוף צפוף. בסנטור קונבנציונאלי אספקת האנרגיה למערכת היא על ידי טמפרטורה או לחץ תהליך זה מתרחש בדרך כלל בטמפרטורה של 80% מטמפרטורת ההיתוך או הפירוק של החומר ונמשכת כסדר גודל של שעות. לצד הסנטור הקונבנציונאלי ישנן שיטות נוספות כגון סנטור בסיוע שדה אלקטרומגנטי.

במהלך סנטור בסיוע שדה אלקטרומגנטי, האבקה או הגוף הירוק נחשפים לשדה אלקטרומגנטי ולטמפרטורה בו זמנית. חשיפה זו גורמת לקצבי סנטור גבוהים יותר בהשוואה לשיטות סנטור קונבנציונאלי וזמן הסנטור נמשך לסדר גודל של דקות ואילו הטמפרטורה הנדרשת יורדת משמעותית, לעיתים עד לשיעור של כ35% מטמפרטורת ההיתוך או הפירוק של החומר. בהנחה שבסנטור באופן זה ניתן לשלוט על מיקרו המבנה של הגוף המסונטר, שיטה זו יכולה לגרום לשיפור בתוכנות החומר כגון שיפור חוזק, העלאה בשקיפות ושיפור הולכה חשמלית, אולם נכון לזמן זה אין תמימות דעים במקורות הספרות לגבי המנגנון או המנגנונים השונים הפועלים בסנטור בסיוע שדה אלקטרומגנטי, והבנתם קריטית על מנת לאפשר את הטמעת שיטה זו.

צורן פחמני (**silicon carbide**) , בשל משקלו הקל, חוזקו הרב וקשיותו הגבוהה יחסית, נפוץ בכלי שחיקה, כלי חיתוך וכן במיגון קרמי בליסטי. בעוד שצורן פחמני בצורתו החד גבישית יכול לשמש כמצע מוליך למחצה, השימוש העיקרי בו הוא בצורתו הרב גבישית. ניתן לסנטר צורן פחמני בשיטות שונות, וברובן מתרחש גידול גרעינים. שליטה בגודל הגרעין ובצורת מיקרו המבנה חשובה לאופטימיזציה של התכונות המכניות. לאחרונה בוצע שימוש בשיטת סנטור בסיוע שדה אלקטרומגנטי על מנת לסנטר צורן פחמני, כאשר אחת הסיבות הייתה טמפרטורת הסנטור הנמוכה בהשוואה לסנטור קונבנציונאלי. התקווה הייתה שסנטור באמצעות שדה יאפשר לסנטר בטמפרטורות נמוכות ובזמנים קצרים יותר וכתוצאה מכך יגרום למיקרו מבנה עדין יותר.

שיטה מרכזית לסנטור בסיוע שדה אלקטרומגנטי, היא שיטת סנטור ניצוץ הפלזמה (**Spark plasma sintering**) או בקיצור האנגלי **SPS**. בעוד ש **SPS** נחקר על מנת לסנטר צורן פחמני לצפיפות מלאה, השפעתו על גידול גרעינים לא נמדדה עדיין. מחקרים מהתקופה האחרונה טוענים כי נוכחות שדה חשמלי מפחיתה את גידול הגרעינים בזירקוניה מיוצבת ע"י איטריה , ומחקרים אחרים טוענים כי סנטור ההבזק (**flash sintering**), שיטת סנטור בסיוע שדה אחרת, יכולה להוריד את שיעור גידול הגרעינים לאפס. בעוד שאין ספק בנוגע לנוכחות של שדה חשמלי ב**SPS**, השפעתו על גידול גרעינים, למיטב ידעתנו, לא נמדדה עד כה. על מנת לעקוב באופן כמותי אחר שינויים בקצב גידול הגרעינים ניתן למדוד ניידות של גבולות גרעין. מטרת עבודה זו הייתה להעריך את ניידות גבולות הגרעינים של צורן פחמני כתוצאה מטיפול תרמי קונבנציונאלי בהשוואה לטיפול תרמי באמצעות **SPS**.

במחקר זה סונטר בתחילה צורן פחמני בשיטה קונבנציונלית ללא לחץ בטמפרטורה של 2100 מעלות צלזיוס באווירת הליום מגנה למשך שעה עד לצפיפות של 94% מהצפיפות התיאורטית. חלקים מהגוף המסונטר נשלחו לטיפולים תרמיים באותו התנור הקונבנציונלי ומתוך כך חולץ גידול הגרעינים כפונקציה של הזמן. במקביל דגימות זהות עברו טיפול תרמי באמצעות **SPS** ללא הפעלת לחץ בטמפרטורה של 2100 מעלות צלזיוס וכן ב1800 מעלות צלזיוס, וגודל הגרעין כפונקציה של הזמן חושב לפי דגמים אלו. הסיבה לטיפולים התרמיים הנוספים ב1800 מעלות הייתה סטיית מדידה אפשרית של הטמפרטורה במכשיר ה**SPS**, והרצון לנטרל את ההשפעה של סטייה זו על מסקנות המחקר.

מתוך ניסויי הטיפולים התרמיים נקבעה ניידות גבולות הגרעין האפקטיבית של צורן פחמני ב2100 מעלות צלזיוס תחת טיפול תרמי קונבנציונאלי ותחת SPS. חימום קונבנציונלי גרם לניידות אפקטיבית של $3.53\cdot10^{-17}$ מטר^2/שניה, ואילו SPS גרם לניידות אפקטיבית של $1.36\text{-}4.79\cdot10^{-14}$ מטר^2/שניה עבור 2100 מעלות צלזיוס תלוי באופי החישוב, ו$6.22\cdot10^{-17}$ מטר^2/שניה עבור 1800 מעלות.

התפתחות מיקרו המבנה במהלך טיפול תרמי ב**SPS** הראתה עליה באנאיזוטרופיות כפונקציה של הזמן, אשר התפתחה מהר בהרבה בהשוואה לטיפול תרמי קונבנציונאלי. בעוד שיחס גובה-הרוחב כפונקציה של הזמן של הגרעינים במהלך הטיפול התרמי הקונבנציונלי לעומת הטיפול בSPS הראו מגמות שונות, כלומר גידול משמעותי בהרבה לטובת ה**SPS**, יחס גובה-הרוחב כפונקציה של גודל הגרעין הראו מגמות זהות.

אם נוכחות השדה החשמלי ב**SPS** אכן משפיעה על גידול הגרעינים, היינו מצפים לראות התאמה בין אוריינטציית הגרעינים וכיוון השדה החשמלי לאחר טיפול תרמי ב**SPS**. אמנם, רעיון זה אינו מתיישב עם תוצאות מחקר זה, אשר איננו מראה התאמה בין כיוון השדה החשמלי ואוריינטציית הגרעינים. אמנם משום שהשדה החשמלי מכוון בכיוון מסוים הוא איננו אמור בהכרח להשפיע על התפתחות מיקרו המבנה באופן אנאיזוטרופי, כך שהיעד התאמה זו אינו שולל את השפעתו של השדה החשמלי על התפתחות מיקרו המבנה.

אף על פי שיחס גובה-הרוחב כפונקציה של זמן הטיפול התרמי אשר הראה שיפוע חד משמעותית עבור טיפול תרמי ב**SPS** על פני טיפול קונבנציונלי, עשוי להוביל למחשבה שהשפעתו של **SPS** הינה אנאיזוטרופית, גודל הגרעינים לאחר טיפול תרמי ב**SPS** היה גדול בהרבה גם כן, והסיבה לאנאיזוטרופיה עשויה לנבוע מגודלם העצום של הגרעינים ולאו דווקא מהשפעת השדה, כלומר תופעה זו עשויה להיות תופעה טבעית של צורן פחמני אשר ניתן להבחין בה באופן ברור רק עבור גידול גרעינים משמעותי.

צורת גרעין המשתנה כפונקציה של הזמן משמעותה שחלק מגבולות הגרעין צריכים להאיץ כפונקציה של הזמן. זה עשוי להעיד על כך שהמערכת לא הגיעה (מגיעה) למצב יציב, כלומר **SPS** גורם לשינוי במנגנון או שינוי סלקטיבי בניידות אשר מונע גידול במצב יציב.

יחס גובה הרוחב כפונקציה של גודל הגרעין הראה שהתפתחות יחס גובה הרוחב בטיפול תרמי קונבנציונאלי וב **SPS** עוקבים אחרי אותה פונקציה, כלומר בדומה ל **SPS**, התפתחות יחס גובה הרוחב במהלך טיפול תרמי איננו מגיע למצב יציב גם כן. ככל הנראה הגרף עבור הטיפול הקונבנציונלי איננו ימשיך באותו שיפוע לעד, ובנקודה מסוימת יתיישר, כלומר יגיע למצב בו יחס גובה הרוחב נשמר קבוע, וככל הנראה **SPS** ימשיך כן באותה המגמה, כפי שניתן להסיק ממיקרו המבנה שהתקבל לאחר טיפול ב**SPS** אשר הכיל גרעינים עצומים. זה מעיד על כך שאותם מגנונים, או מנגנונים דומים, אשר מקדמים סנטור מהיר במהלך SPS גם מגדילים משמעותית את שיעור גידול הגרעינים, או שצורת הגרעינים לא הגיעו למצב עמיד כאשר בוצע שימוש ב**SPS**.

סיבה אפשרית להבדלים בקצב ו/או באופן התפתחות מיקרו המבנה בין שתי שיטות הטיפול התרמי יכול לנבוע מההבדל באופן החימום בשתי השיטות. בעוד שהחימום בתנור הקונבנציונלי מתבצע על ידי הסעה על פני השטח, ב**SPS** החימום נובע מהזרם הזורם בחלקו דרך הכורית העוטפת את הדגם ובחלקו דרך הדגם עצמו. הגוף ב**SPS** ממוקם באופן מקביל מבחינה חשמלית עם הכורית, ובעוד שרוב הזרם עובר דרך הכורית העשויה גרפית בעלת התנגדות חשמלית נמוכה, חלק מהזרם זורם אף דרך הדגם. הזרם הקטן אשר זורם דרך הדגם, זורם בעיקרו במסלולים בעלי התנגדות חשמלית נמוכה כלומר דרך גבולות גרעין. זרם זה מחמם חימום ג'אול במסלולו, וחימום זה עשוי להשפיע על ניידות גבולות הגרעין בדרכים שונות: הוא יכול להגביר את הדיפוזיה בגבולות הגרעין, או שבאמצעות מספיק אנרגיה הוא יכול לבצע מעבר קומפלקשן אשר עשוי להגביר את ניידות גבולות הגרעין.

התופעות שנצפו בהתפתחות מיקרו המבנה לאורך הטיפול התרמי ב**SPS** ב2100 מעלות צלזיוס, לא נצפו ב1800 מעלות צלזיוס ב**SPS**. היעדר תופעות אלו עשוי להצביע על קיום נקודת סף כלשהי אשר ממנה מותנעים מנגנון או מנגנונים שונים לצד המנגנונים שכבר פועלים בהתפתחות מיקרו המבנה במהלך טיפול תרמי קונבנציונאלי. מחקר מעמיק יותר על נקודות נוספות בטמפרטורות שונות בין 1800 ל 2100 מעלות צלזיוס עשוי לשפוך אור על קיומה של נקודת סף זו.

במחקר זה הראנו באופן ברור שטיפול תרמי ב**SPS** בו שדה חשמלי נוכח כמעט באופן תמידי, הגדיל באופן משמעותי את ניידות גבולות הגרעין (שלושה סדרי גודל). זה בניגוד לפירוש של תוצאות שדווחו בספרות. בעוד שמחקרים המופיעים בספרות מראים תוצר של מיקרו מבנה עם גרעינים עדינים יותר בנוכחות שדה חשמלי, ומתוך כך מסיקים כי שדה חשמלי מאט גידול גרעינים, הבעיה עם מסקנות אלו היא שהמדידות של גבולות הגרעין בוצעו בזמן שהתרחש סנטור. במהלך סנטור מתרחשים תהליכים נוספים מלבד גידול גרעינים, כמו ציפוף אשר עשוי להשפיע גידול גרעינים, ולכן מסקנות אלו בנוגע להשפעת שדה חשמלי על גידול גרעינים הוסקו שלא כהלכה.